CHALMERS
UNIVERSITY OF TECHNOLOGY

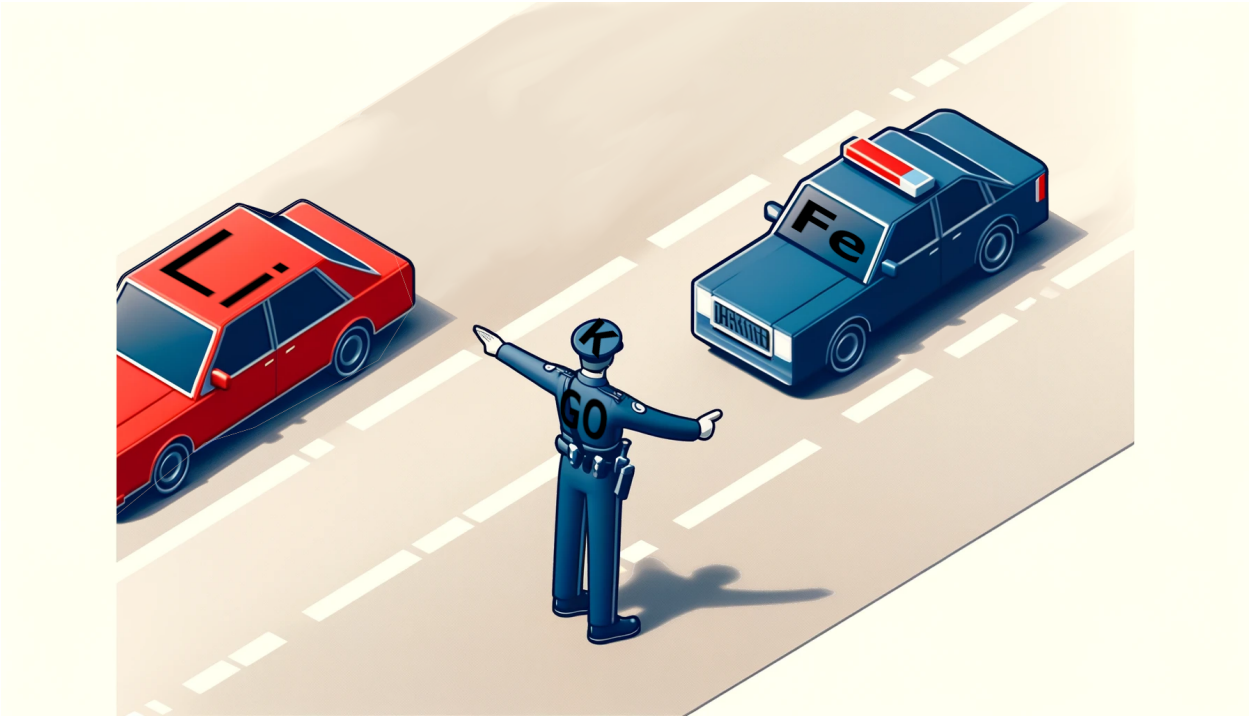


# Graphene oxide based ion-sieving membranes for water purification

Master's thesis in Microtechnology and nanoscience

Michał Maciałowicz

DEPARTMENT OF INDUSTRIAL AND MATERIALS SCIENCE
CHALMERS UNIVERSITY OF TECHNOLOGY
Gothenburg, Sweden 2024
www.chalmers.se

Master's thesis 2024

# Graphene oxide based ion-sieving membranes for water purification

Michał Maciałowicz


CHALMERS
UNIVERSITY OF TECHNOLOGY

Department of Industrial and Materials Science
Chalmers University of Technology
Gothenburg, Sweden 2024

Graphene oxide based ion-sieving membranes for water purification
Michał Maciałowicz



Supervisor: Dr. Zhenyuan Xia, Department of Industrial and Materials Science
Examiner: Prof. Uta Klement, Department of Industrial and Materials Science

Master's Thesis 2024
Department of Industrial and Materials Science
Chalmers University of Technology
SE-412 96 Gothenburg
Telephone +46 31 772 1000

Cover: AI-generated image (using GPT-4o model) symbolically depicting potassium intercalated graphene oxide layer selectively blocking specific ions.

Typeset in LaTeX
Gothenburg, Sweden 2024

Graphene oxide based ion-sieving membranes for water purification
Michał Maciałowicz
Department of Industrial and Materials Science
Chalmers University of Technology

# Abstract

Graphene oxide (GO), a promising two-dimensional (2D) material, has attracted much attention in membrane filtration techniques such as selective ion filtration and contaminant removal in water treatment. However, its versatility is limited by the fact that GO-based membranes tend to swell when submerged in water. This swelling behaviour will lead to an expansion of the 2D interlayer space, resulting in their inability to block particles in subnano-scale. In this thesis, I studied the modification of GO membrane to fine-tune the 2D interlayer distance and tested the ion-selectivity behaviour of modified GO membrane in lithium ion extraction applications. The impact of functional groups on GO membrane was evaluated by X-ray diffraction, Raman spectroscopy, and scanning electron microscopy measurements. This work will provide a simple strategy in the development of emerging filtering materials for water purification applications.

Keywords: 2D-nanomaterials, graphene oxide, ion sieving, water treatment.

# Acknowledgements

I would like to take this opportunity to express my most sincere gratitude towards my supervisor Zhenyuan Xia for his continuous support and patience which were indispensable to me during this past semester and without which this thesis could not have been completed.

Michał Maciałowicz, Gothenburg, June 2024

# List of Acronyms

Below is the list of acronyms that have been used throughout this thesis listed in alphabetical order:

| | |
|---|---|
| 2D | Two-dimensional |
| Arg | Arginine |
| DI | deionized |
| ICP-OES | Inductively Coupled Plasma Optical Emission Spectroscopy |
| Lys | Lysine |
| LFP | Lithium Iron Phosphate |
| Glu | Glutamate |
| GO | Graphene oxide |
| SEM | Scanning Electron Microscopy |
| XRD | X-ray diffraction |

# Contents

# List of Figures

# List of Tables

# 1
# Introduction

The first successful synthesis of graphene reported in 2004 [1] was without a doubt a milestone in the area of nanotechnology. The significance of this discovery lies in the fact that, for the first time, it proved experimentally the possibility of creating thermodynamically stable films with a sub-nanometer thickness. This possibility opened up the way for the development of other two-dimensional (2D) materials. These nanomaterials have many exciting potential applications, including field-effect transistors, gas sensors, high strength composites and many others [2].
Graphene oxide (GO) is one of many such 2D materials developed in recent years. Unlike its "parent-material" graphene, GO is hydrophilic. This makes it much easier to handle for many applications, specifically - membrane preparation. When flakes of GO are stacked on top of each other, they form nanochannels, with interlayer spacing reaching sub-nanometer values [3, 4]. Molecules with sizes larger than the interlayer spacing cannot easily penetrate such barrier which leads to the possibility to develop membranes capable of precise and efficient sieving of molecules as small as few ångströms [4, 5]. These type of devices show great promise and have been tested in variety of different uses, such as power generation [6], managing nuclear waste [4], water desalination and purification [5, 7, 8], proton conductors [5], energy storage [5], gas separation [5] and ion separation [5].
It is important to note however, that GO membranes submerged in an aqueous solution tend to swell up, increasing their interlayer spacing to $\sim$13 Å [3, 5]. This makes it impossible for pure GO membrane to block out sub-nanometer particles dissolved in water and hinders the potential application of such membranes in separation of smaller ions. To remedy this problem, various modification methods are being investigated with the goal of increasing stability of GO membranes and creating efficient ion-sieving devices.

## 1.1 Background

With the environmental concerns growing ever stronger, there is a large push in the transition from conventional to electric vehicles. It is expected that by 2030, 7% of all vehicles present on the roads will be electric. Moreover, this ratio is expected to increase even further, reaching a situation in which half of the vehicles become electric in 2040 [9]. This in turn must naturally lead to an increase in the demand for batteries necessary to power so many cars.
One example of batteries which are considered to be the right candidate for this purpose are lithium iron phosphate (LFP) batteries. This choice is motivated by

their excellent properties ranging from high theoretical capacity and energy density to high reversibility and thermal safety [10]. However they still have a limited lifetime and eventually need to be exchanged for new ones and recent forecasts state that the number of depleted lithium-ion battery packs per year will reach 1 000 000 in 2030.
Lithium is considered to be the most valuable element present in LFP batteries [11]. However, current techniques for lithium extraction are mainly based on hydrometallurgy treatment, which needs harsh chemicals and consumes large amount of water during the process. Moreover, it can bring potential contamination to the aquatic ecosystem. Therefore, improving the processes used to extract it, either from natural sources or depleted batteries, is going to be a vital task moving forward. To that end, the ion separation capability of graphene oxide membranes appears to be a promising avenue for research.

## 1.2 Scope and overview

The main purpose of this thesis is to study the modification of GO membranes to fine-tune the 2D interlayer distance. Additionally the ion selectivity behaviour of modified GO membranes will be tested in lithium ion extraction applications. The effects of several modification methods on the membrane properties will be investigated and compared between one another. The aim is to establish which of them is best suited for the aforementioned extraction application.
The lithium ion extraction capability will only be studied on a laboratory scale, i.e. in the milliliter range. No experiments scaled-up to the level of liters will be performed to prove the usability of presented method in practical conditions. Measurements of occurring to membrane properties after multiple cycles of operation were also not performed.

# 2
# Theory

## 2.1 Graphene

In order to give a good explanation of the properties and behaviour of GO, it might be a good idea to first talk a little bit about its "parent material" - graphene. Graphene is one of the allotropic forms of carbon, just like fullerenes, diamonds or graphite. Actually, graphene has a lot in common with graphite, since, strictly speaking, graphene in its pristine state is a single, atomically thin sheet of graphite. In order to better illustrate the relation between graphene and graphite, several graphene sheets stacked on top of each other forming graphite are depicted in Figure 2.1.

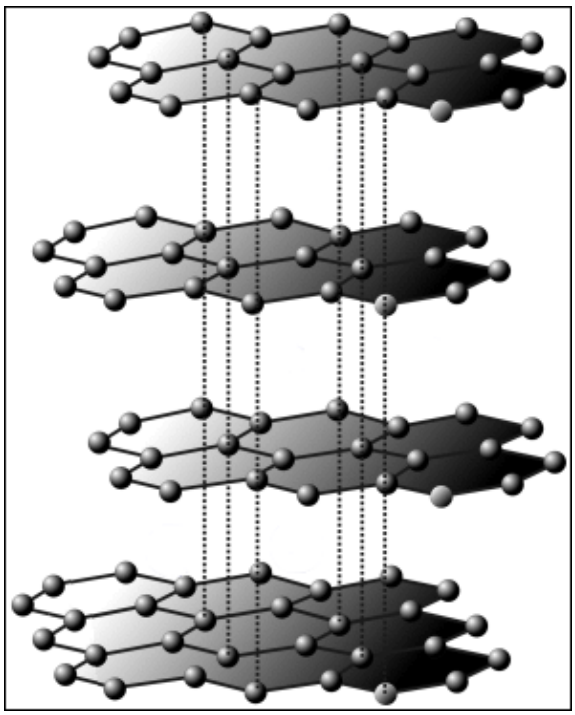

**Figure 2.1:** The relation of graphene to graphite. (2009). CC BY-SA 2.5 [12]

Carbon atoms in graphene are arranged in a hexagonal lattice, often likened to a "honeycomb" or "chicken-wire" structure. These atoms are bonded together by strong $\sigma$ bonds with a length of 0.142 nm [13]. The remarkable mechanical strength, a Young modulus of 1.0±0.1 TPa and an ultimate tensile strength of 130±10 GPa, of graphene is attributed to the presence of these exact same $\sigma$ bonds [14]. The $\sigma$ bonds

between carbon atoms are created by $2s$, $2p_x$ and $2p_y$ electron orbitals hybridized into $sp^2$ hybrid orbitals [13], which accounts for 3 out of 4 valence electrons of graphene. The last one, in the form of a $\pi$ orbital, can move freely along a graphene sheet, and is responsible for its electronic properties [13]. These properties include not only an electrical conductance of $10^6$ S/cm but also occurrence of a quantum Hall effect and electrons behaving as massless Dirac fermions [14]. For clarity, the structure of hybridized orbitals in graphene are shown in Figure 2.2.

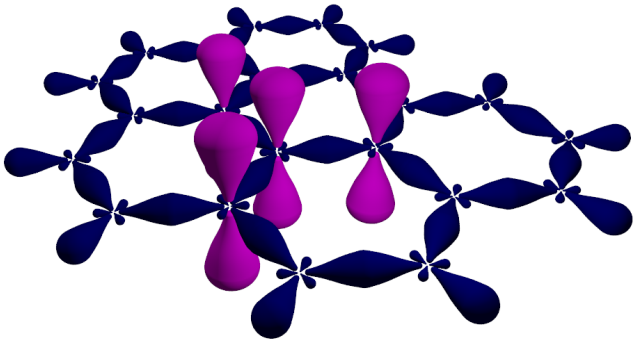

**Figure 2.2:** Hybridized orbitals present in a graphene sheet. (2020). CC BY-SA 4.0 [15]

## 2.2 Graphene oxide

Now, with the better understanding of the nature of graphene, we can start talking about GO, the main material of interest for the purpose of this thesis. As its name suggests, GO is an oxidized form of graphene. Strongly reactive, oxygen-containing functional groups bind to the hexagonal lattice, introducing defects into the crystal structure. An example of what a graphene oxide structure can look like is shown in Figure 2.3. Many theoretical models have been put forward with the aim of describing exactly what types of defects are produced in this manner. These include carbonyl, carboxyl and hydroxyl groups. They can be present at the edges of the materials as well as randomly distributed on its surface disrupting the aromatic structure [16]. Additionally, some of the newer models account for the possibility of hole defects present due to over-oxidation [16].
One of the most important properties of 2D materials is the fact that majority of their atoms, or in the case of graphene and GO all of their atoms, are present at the surface. This means that surface functionalization can drastically change all of their properties, which is very different to how more conventional 3-dimensional bulk materials operate. In the case of graphene, the presence of defects is caused by the oxidation. While GO is actually an insulator [18] and its Young's modulus drops to below 500 GPa [19, 20]. Moreover, some of its most exotic properties, e.g. quantum Hall effect are no longer being reported in sheets with as many defects. However, this does not mean that GO is an inferior form. The high specific surface area remains close to graphene [21]. Moreover, in exchange for the properties that GO looses due

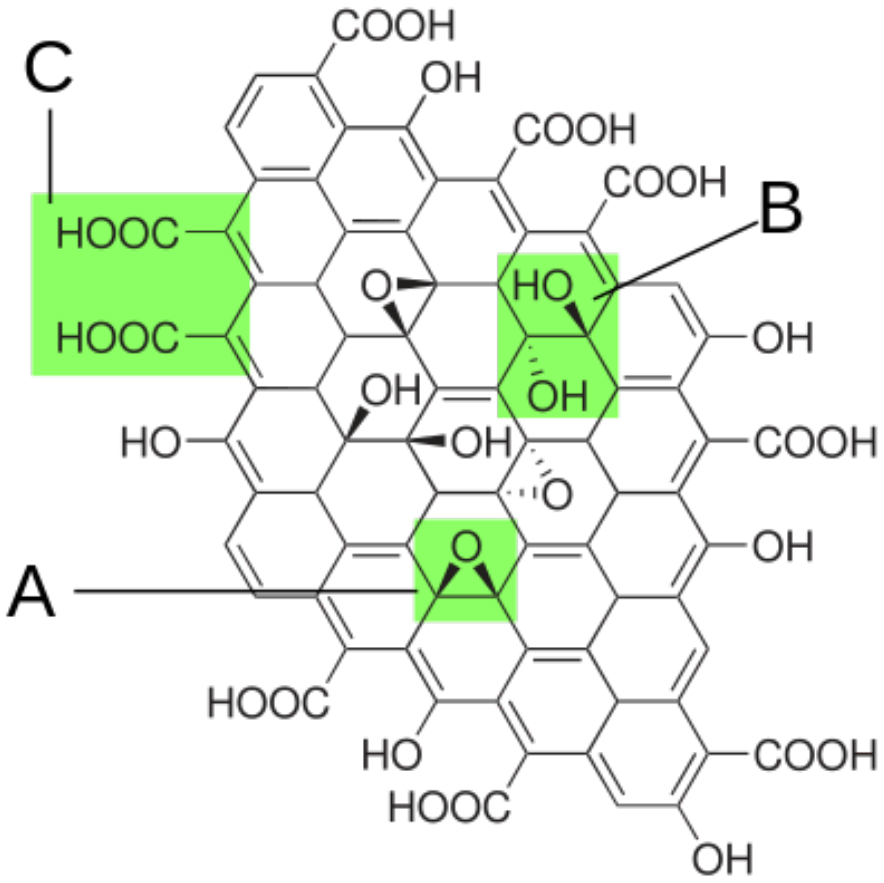


**Figure 2.3:** Chemical structure of graphene oxide (GO). (2012). Public Domain via Wikimedia Commons. [17]
Three different functional groups which can be present in GO sheets are: A) epoxy group B) hydroxyl group C) carboxyl group.

to defects in the crystal lattice, it becomes much more chemically active. Unlike the purely aromatic graphene, many defects present on the GO offer an opportunity for easy functionalization with a variety of chemical groups. Additionally, GO becomes hydrophilic, making it possible to be prepared and handled in an aqueous solution with ease.

The measurable spacing between layers also increases upon oxidation. While single layer graphene sheets are usually reported to be separated by a distance of 0.335 nm [22], GO sheets increase their distance up to ∼0.8 nm [5]. This increase in thickness, combined with hydrophilic nature of oxygen containing groups, form the foundations for the most common approach to GO synthesis, the so-called *Hummers' method* [23]. This method consists of 2 distinct steps. Firstly, graphite crystals are treated with strong oxidizing agents. This, as explained above, introduces oxide groups in-between the sheets of graphite, causing the material to expand. This procedure forms

**Table 2.1:** Hydrated atomic radii of some selected ions [26].

| Ion | Hydrated radius (nm) |
|---|---|
| $K^+$ | 0.331 |
| $Li^+$ | 0.382 |
| $Ni^{2+}$ | 0.404 |
| $Cu^{2+}$ | 0.419 |
| $Co^{2+}$ | 0.423 |
| $Mg^{2+}$ | 0.428 |
| $Mn^{2+}$ | 0.438 |
| $Fe^{3+}$ | 0.457 |
| $Al^{3+}$ | 0.475 |

an intermediate material known as graphite oxide. Next, graphite oxide is exfoliated into GO form. Because the distance between the graphite oxide sheets increases compared to graphite, the interactions keeping the material together weaken, making the exfoliation process to require much less energy [24]. Thanks to the hydrophilicity of GO, liquid phase exfoliation in water does not run into the risk of reaggregation of flakes, which can happen during the exfoliation of graphene. Because of the low cost and ease of large scale production of GO it is often also used as a precursor in the production of reduced graphene oxide - an intermediate for of material between graphene and graphene oxide.

## 2.3 Ion-sieving membranes

As was alluded to in previous sections, when sheets of a 2D material are stacked on top of one another, thin channels, whose sizes can reach sub-nanometer level, are formed between them. These *nanochannels*, as they are sometimes called, can be utilized to construct the eponymous ion-sieving membranes. A qualitative explanation of the mechanism responsible for the ion-sieving behaviour is rather straightforward. Its foundation lies in the size exclusion effect, also known as a steric exclusion effect. It means that molecules, whose diameters are larger than the interlayer distance will find it much more difficult to traverse the membrane. This principle has been shown to work well for example in gas separation applications [5].
In the case of ions in an aqueous solution, the situation becomes a little bit more nuanced. This is because of an effect called *hydration* which can happen to ions. Due to their non-neutral electrical charge, ions in water experience electrostatic interaction with water molecule dipoles. This interaction causes the water dipoles to arrange themselves around the ions in a shell-like manner, effectively increasing their radius [25].
A comparison of hydrated radii of a few selected ions is presented in Table 2.1
To explain it further, ion hydration is an effect reminiscent of the formation of double layer upon the presence of surface charge. When ions of a crystalline salt separate, the dipoles of water cluster around each one of them, forming the aforementioned shells. These shells screen oppositely charged ions from attractive forces which would

normally cause them to coalesce back together [25].
Notably the hydrated ions can pass through a membrane even when their hydrated radius is larger than the interlayer distance of the lamellar structure. This can happen thanks to a so-called *partial dehydration* [27]. Some or all of the water molecules can get detached from the ion-water complex upon its entry into the nanochannels. This means that even if a size of a nanochannel is fixed to be lower than the hydrated radius of an ions which are desired to stop, some of them can still traverse the membrane. There is however an energy barrier to this process, provided by the lowering of potential energy which occurs when ions and water molecules come close together forming a hydrated complex. Due to this, ions with higher amounts of charges are expected to need more energy in order to traverse such membranes [28]. Additionally, it has been shown by molecular dynamics simulations that the permeation rate should scale exponentially with decreasing channel size [28].
While the steric exclusion is considered to be the main factor responsible for slowing down the permeation rate of ions [3, 29], it turns out, that the rejection performance of membranes based on 2D materials is also dependent on another effect. The sieving of ions happens not only because of their size, but also due to their electrical charge [29, 30]. Analogously to biological ionic channels, the presence of electrical charge exerts repulsive force on incoming ions of the same sign [30].

## 2.4 Swelling

Now that both the material itself as well as membranes' principle of operation have been sufficiently explained, the time has come to tackle the main issue, first mentioned in the introduction section. Unfortunately, it turns out that the same hydrophilic nature of GO which made it easier to synthesise and handle is actually a double-edged sword when it comes to ion sieving membranes. The affinity of water molecules towards the oxide groups causes the former to penetrate deep into the lamellar structure, as depicted in Figure 2.4.
The amount of water which accumulates inside nanochannels is enough to force the GO sheets apart, increasing the interlayer spacing. According to the definition, such expansion caused by an uptake of another substance is called *swelling* [32]. This property to expand when submerged under water has been the reason why preparing membranes with sufficiently small spacing to exclude ions has been challenging [5]. Tendency to swell is so characteristic of GO, that some authors have suggested to use this property as a defining trait, distinguishing GO from less functionalized derivatives of graphene which do not uptake water [32].
A typical distance between GO sheets stacked on top of one another is equal to 7.9 Å [3]. However, as was explained in the introduction, swelling can cause it to increase up to ∼13 Å [3]. Comparing this value with the hydrated radius presented in Table 2.1 makes it clear that membranes expanded in this manner no longer posses the ability for steric exclusion.
Notably, this swelling behaviour is not unique to GO. As a matter of fact, it is a common problem in membranes assembled from 2D materials [27]. It occurs whenever we are dealing with with atomically thin, hydrophilic sheets stacked on top of each other. For example, oxygen terminated MXenes face the same adversity [27].

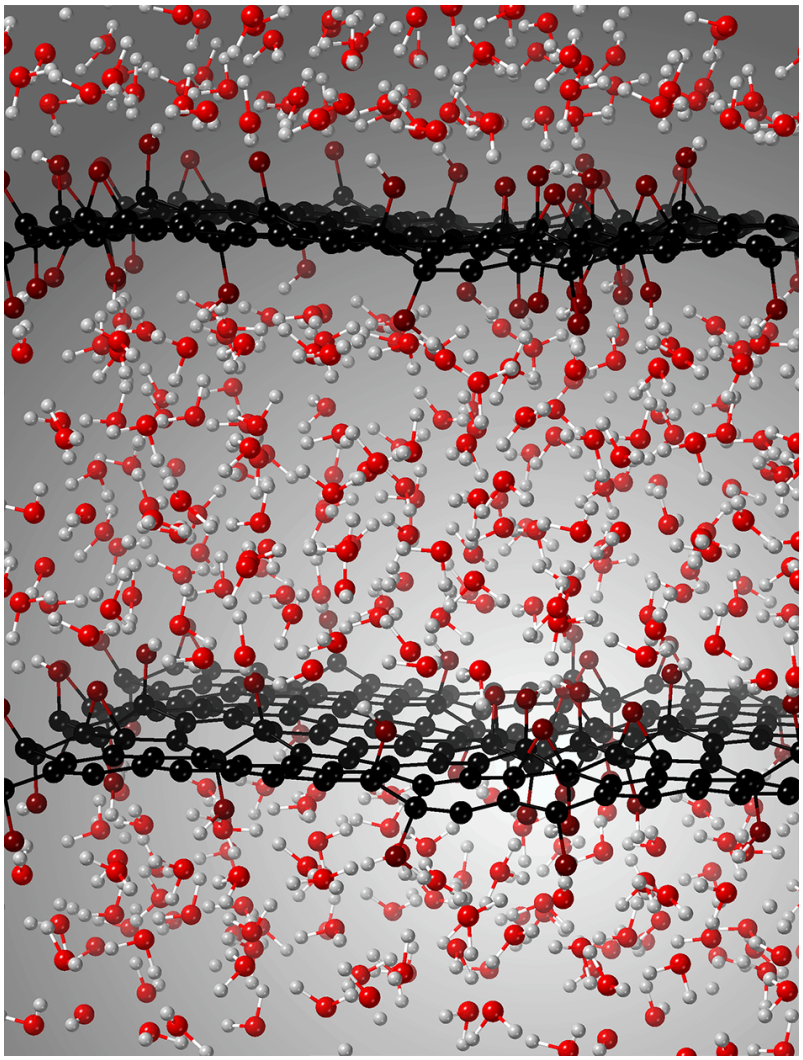

**Figure 2.4:** Snapshot of graphene oxide in liquid water from molecular dynamics simulation. (2020). CC BY 2.0 [31]

Therefore, finding effective methods of increasing membrane stability and tuning the interlayer distance to the correct size is crucial in development of ion-sieving devices from such materials.

## 2.5 Swelling prevention

A possible approach to address the pressing issue of nanochannel expansion is to utilize crosslinking. The idea is to decorate GO sheets with additional functional groups with the aim of connecting them at a fixed distance and preventing them from swelling under water. Naturally, any such binding will have to be strong enough to overcome the hydrogen bonding between the water dipoles and oxide groups of the GO. To that end, some approaches utilizing covalent functionalization have already been reported [33]. Using density functional theory simulations Yuan et al. [33] managed to show that GO sheets functionalized with polyethylenimine

connect with each other through a network of hydrogen bonds. These bonds make them stable in the presence of water.
Another approach is to intercalate a GO membrane with metal ions. Using molecular dynamics simulations, Chen et al. [5] managed to show that hydrated cations can play a role of a crosslinker. These positively charged ions travel towards places on the GO sheet where aromatic rings meet the oxide groups. The water molecules surrounding the cations form hydrogen bonds with GO sheets which were calculated to be around 30 times stronger than those formed between GO sheets and pure water. Moreover, this crosslinking behaviour is intensified by *cation-*$\pi$ interactions [5]. They are based on electrostatic attraction between positively charged cation and a negatively charged electron cloud of the aromatic structure. Much like hydrogen bonding and $\pi - \pi$ stacking, cation-$\pi$ interactions are an example of a non-covalent interaction. As a matter of fact, cation-$\pi$ interactions are considered to be the strongest of these 3 types [34]. This makes them a promising strategy to counteract the swelling behaviour mediated by hydrogen bonds.
Additionally, cation intercalation provides and additional advantage. By filling the GO nanochannels with positively charged ions, it introduces a repulsive force towards other ions with the same charge. This happens even though the nanochannels were originally negatively charged [3].

# 3
# Methods

## 3.1 Membrane preparation

The membranes were prepared using a facile vacuum filtration method. Firstly, 0.2 mg of GO powder (< 35 mesh, purchased from Abalonyx) was dissolved in 20 ml of deionized (DI) water and sonicated for a total of half an hour. Next, this solution was filtered through a cellulose acetate membrane, which was previously wetted with DI water. This filtration was performed using an experimental setup visible in Figure 3.1, connected to the vacuum. The cellulose acetate membrane used was and OE 66 membrane purchased from Cytiva with a pore size of 0.2 $\mu$m and a diameter of 47 mm. After the entirety of the solution passed through leaving a GO deposit on top, the GO membrane was placed between two pieces of glass and left to dry in the oven in ambient atmosphere at 60°C for around and hour.

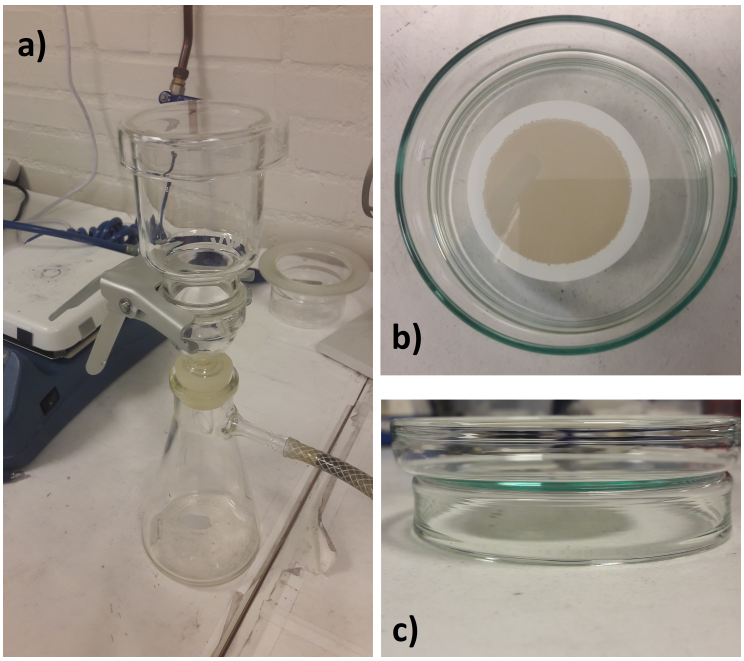


**Figure 3.1:** Experimental setup for membrane preparation. a) Cellulose acetate membrane ready for vacuum filtration b) filtered membrane between 2 pieces of glass (top view) c) filtered membrane between 2 pieces of glass (side view).

Additionally, for the purpose of later XRD measurements, two more types of membranes were prepared.

One of them had the GO loading increased to 2 mg. It was prepared in the same manner as above - dissolved in 20 ml of DI water with the concentration increased by 10 times, sonicated for half an hour and filtered through a cellulose acetate membrane.

The second one was a freestanding membrane. In this case, 0.5 ml of a 5 mg/ml GO solution (prepared from the same GO powder) was dropcasted onto a teflon strip. A drop was then left in the oven at 60°C in ambient atmosphere until it was completely dry. Lastly, the as prepared membrane was peeled off using tweezers.

A comparison of all 3 types of membranes is shown in Figure 3.2.

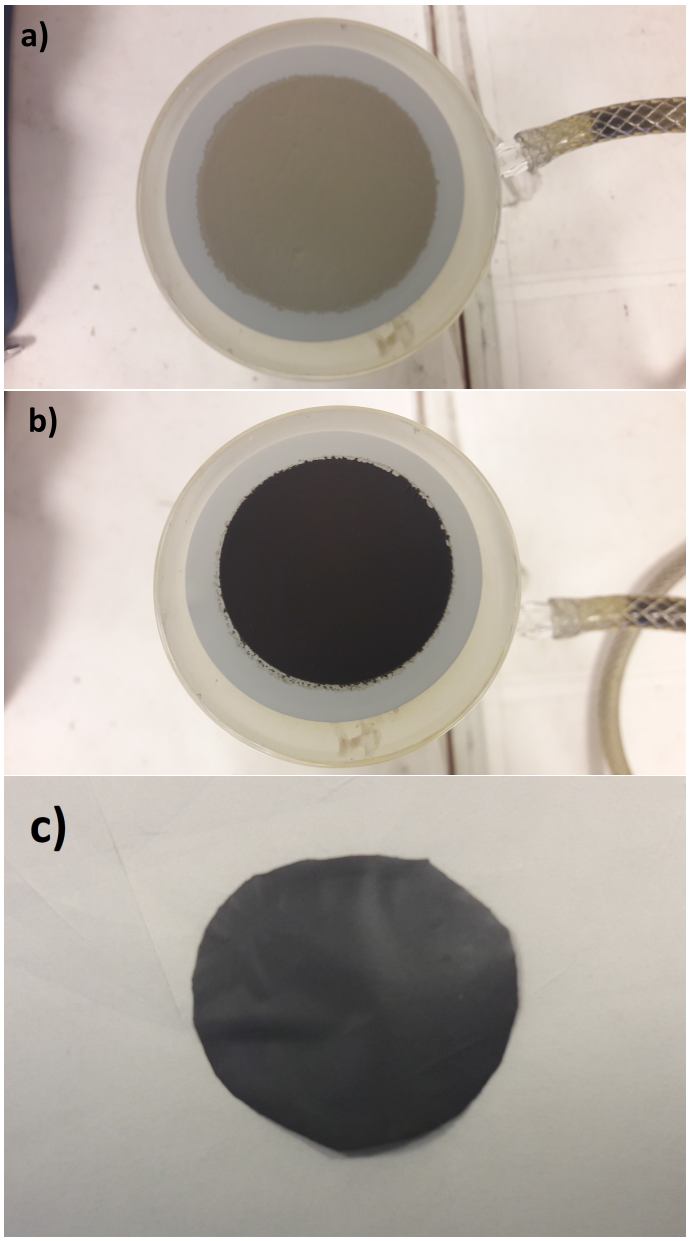


**Figure 3.2:** Three types of membranes side by side. a) 0.2 mg loading b) 2 mg loading c) freestanding.

## 3.2 Membrane characterization

The membranes were characterized using three different techniques:

- Raman spectroscopy
- Scanning electron microscopy (SEM)
- X-ray diffraction (XRD)

The Raman spectroscopy measurements were performed on horizontally placed membranes using a WITec alpha300 R device.
For the SEM measurements, the membranes were first frozen with liquid nitrogen and cut in smaller pieces in order to obtain information about the cross-section. The measurements were performed with the JEOL JSM-7800F Prime device after the samples were sputtered with gold using LeicaEM ACE600. The accelerating voltage used during all of the measurements was 5 kV
The XRD measurements were performed with the D8 Discover X-ray diffractometer from Bruker operating in the standard Bragg-Brentano configuration. In order to see how the intercalation affects the membranes, samples were cut into three pieces each. One of the pieces was measured in a dry state, while the other two underwent an additional treatment. One of these two was immersed in a 1.5 M aqueous solution of KCl for half an hour right before the measurements. The other was immersed for the same amount of time in pure DI water instead. It served as a reference, to observe the effects of swelling.

### 3.2.1 Raman spectroscopy

Raman spectroscopy is a characterization method popularly used in condensed matter applications. It is based on the *Raman scattering*, i.e. a type of inelastic light scattering which can occur once specific conditions are met [35].
Raman scattering occurs when an incoming photon of light causes a creation (or annihilation) of a phonon, a quasiparticle made of collective vibrations of atoms in the absorbing material. The energy of this phonon is removed (or added) to the scattered photon, causing its wavelength to shift [35].
Raman scattering can only occur for very specific wavelengths of light, depending on the symmetry groups of the crystal structure of a material under investigation. Therefore, any changes to such structure, will be reflected in the spectrum of scattered light. This is why, this method is so well suited for detecting oxidation of graphene into GO, which introduces many defects into the crystal structure, significantly impacting its symmetries [35].

### 3.2.2 Scanning electron microscopy

SEM, as its name suggests, is a microscopy method, in which electrons are used to probe a sample under investigation, instead of photons, which are used in a more traditional optical microscopy. The advantage of such approach comes from the fact that electrons accelerated to high energies (above 2 keV) have very short wavelengths (on the order of picometers) [36]. This allows for the resolution of very fine morphological features of the material under investigation.

A beam of electrons coming from an electron gun (e.g. made up of a lanthanum hexaboride crystal) pass through a carefully controlled electromagnetic field which acts as a replacement to the optical lenses used in light-based microscopes [36]. In order to prevent unwanted scattering, the electrons travel the distance from the electron gun to the measured samples through a vacuum [36].
As will be later seen in the results section, SEM is an irreplaceable technique offering great insight into the morphology of nanoscopic samples under investigation.

### 3.2.3 X-ray diffraction

XRD is a measurement method typically used to obtain information about distances between crystal planes in solid state samples. This method is based on the so-called *Bragg's condition* for reflection. It describes a relation between the integer multiples of the wavelength of incident light ($n \cdot \lambda$), distance between crystallographic planes ($d$) and the angle of incoming light ($\Theta$), as shown in Equation 3.1 [37].

$$n \cdot \lambda = 2 \cdot d \cdot \sin \Theta \tag{3.1}$$

More advanced experiments utilizing XRD can get rather complicated, however, in the simplest case, X-ray source and the X-ray detector are both kept at an angle $\Theta$ from the surface of the measured sample [37].
Substituting a position of a given peak for $\Theta$ in the Equation 3.1 allows one to calculate a distance for the corresponding spacing.

## 3.3 Permeation tests

In order to quantify the permeation rates of ions, the membranes were tested with the experimental setup presented in Figure 3.3. Investigated membrane was placed between the two glass tubes, one of which was filled with DI water and the other with a salt solution containing investigated ions. These ions included $Li^+$ and $Fe^{3+}$. In the case of the former the glass tube was filled with a 0.1 M solution of LiCl (purchased from VWR Chemicals BDH) while in the case of the latter, with a 0.1 M solution of $FeCl_3$ (purchased from Sigma-Aldrich in an anhydrous form). The permeation tests lasted for 2 h each. During that time, the conductance was continuously measured on the side of initially DI water using the PC 8+ DHS Multiparameter manufactured by XS Instruments.
After the initial period of stabilization, the permeation rates were calculated from the data obtained in the last hour using the equation 3.2.

$$P = \frac{V}{A}\frac{\Delta C}{\Delta t} \tag{3.2}$$

Where:

- $P$ - permeation rate
- $V$ - volume of the solution on one of the sides
- $A$ - area of the membrane in contact with the solutions
- $\frac{\Delta C}{\Delta t}$ - slope of a concentration vs time curve

**Figure 3.3:** Experimental setup for permeation tests.

Additionally, ionic selectivity, i.e. a ratio of permeation rates of two different ionic spices, was also calculated

In order to evaluate the effect of ion intercalation on the above quantities, GO membranes were first immersed in a 1.5 M solution of KCl (purchased from EMSURE) for half an hour. Afterwards, it was taken out, gently dried with a tissue and placed between two pieces of glass and left in the oven at 60°C in ambient atmosphere for half an hour. Afterwards it was rinsed and immersed in fresh DI water for another half an hour to remove excess potassium ions. As the last step, the membrane was once again placed between two pieces of glass and left in the oven for half an hour. The membranes prepared in such manner were subsequently also put to the permeation test described above.

To be able to calculate concentration from conductance, calibration curves for LiCl and $FeCl_3$ were prepared in the following manner. Firstly, a 0.1 M solution of an investigated salt was prepared and its conductance was measured. Then, the solution was diluted in half and its new conductance was recorded again. This process was repeated until the conductance reached levels of pure, DI water, i.e. $\sim$1 $\mu$S/cm.

## 3.4 Additional membranes

Apart from the membranes prepared on site, the above measurements were also performed on a series of GO membranes prepared in the ISOF institute in Bologna, functionalized with the following chemicals:

- Arginine (Arg)
- Lysine (Lys)
- Glutamate (Glu)

as well as pure GO membranes prepared there as well as a reference. Molecular graphs of these three chemicals are presented in Figure 3.4.

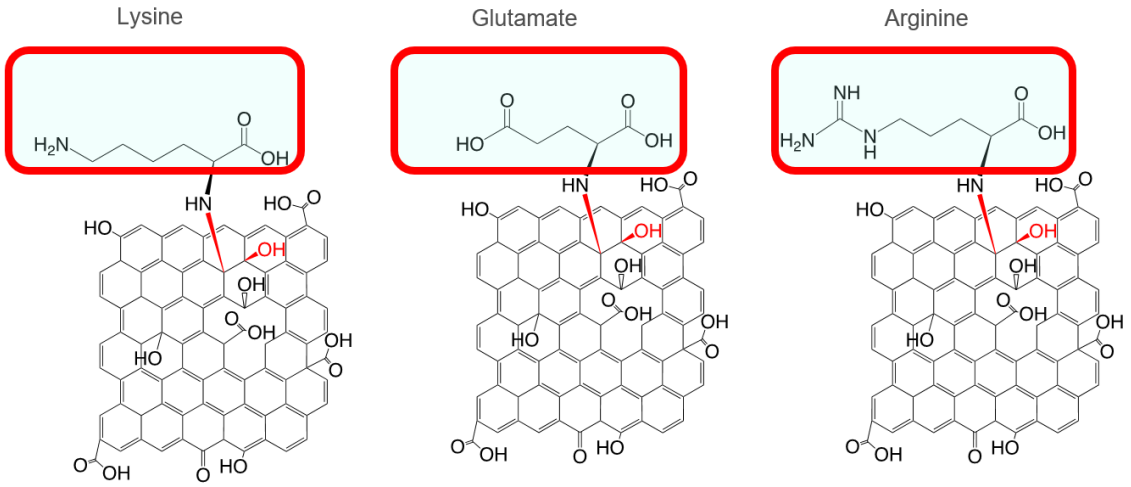


**Figure 3.4:** Molecular graphs of GO functionalized with Arginine, Lysine and Glutamate.

The membranes mentioned above were prepared from 1-to-1 mixtures of pure GO and GO functionalized with a given chemical, and are therefore going to be referred in the rest of this thesis as GO+Arg/GO, GO+Lys/GO and GO+Glu/GO.

# 4

# Results and discussions

## 4.1 Raman spectroscopy

First of all, the Raman spectra of membranes prepared on site are shown in Figure 4.1. Moreover, the Raman spectra of GO membranes from ISOF are presented in Figure 4.2.

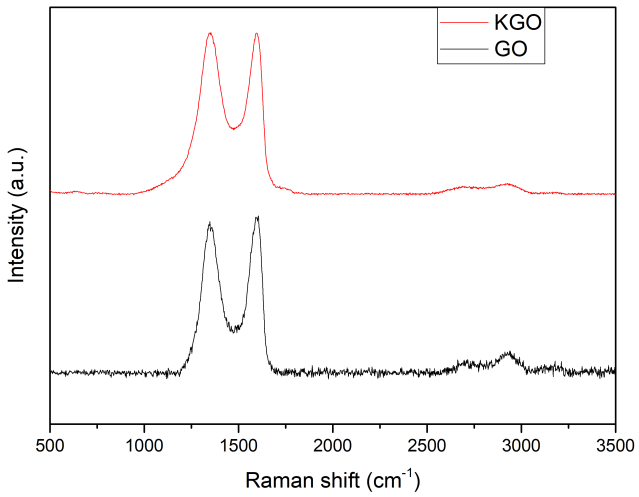


**Figure 4.1:** Comparison of the Raman spectra of 2 mg GO and potassium intercalated (KGO) membranes.

Using WiRE 5.1 software from Renishaw, peaks were fitted to the Raman data presented above. Using these fits, peak positions were extracted to evaluate the quality of the utilized graphene oxides. Values for the extracted peaks are presented in Table 4.1. These values are consistent with those found in literature. The D peak position reported in other works ranges from 1345 to 1363 $cm^{-1}$ wheres G peak position ranges from 1584 to 1605 $cm^{-1}$ [38–42]. Moreover, given the relatively small changes to peak positions, it appears as though the investigated methods of GO modification do not have any drastic effect on the crystallographic structure of the materials.

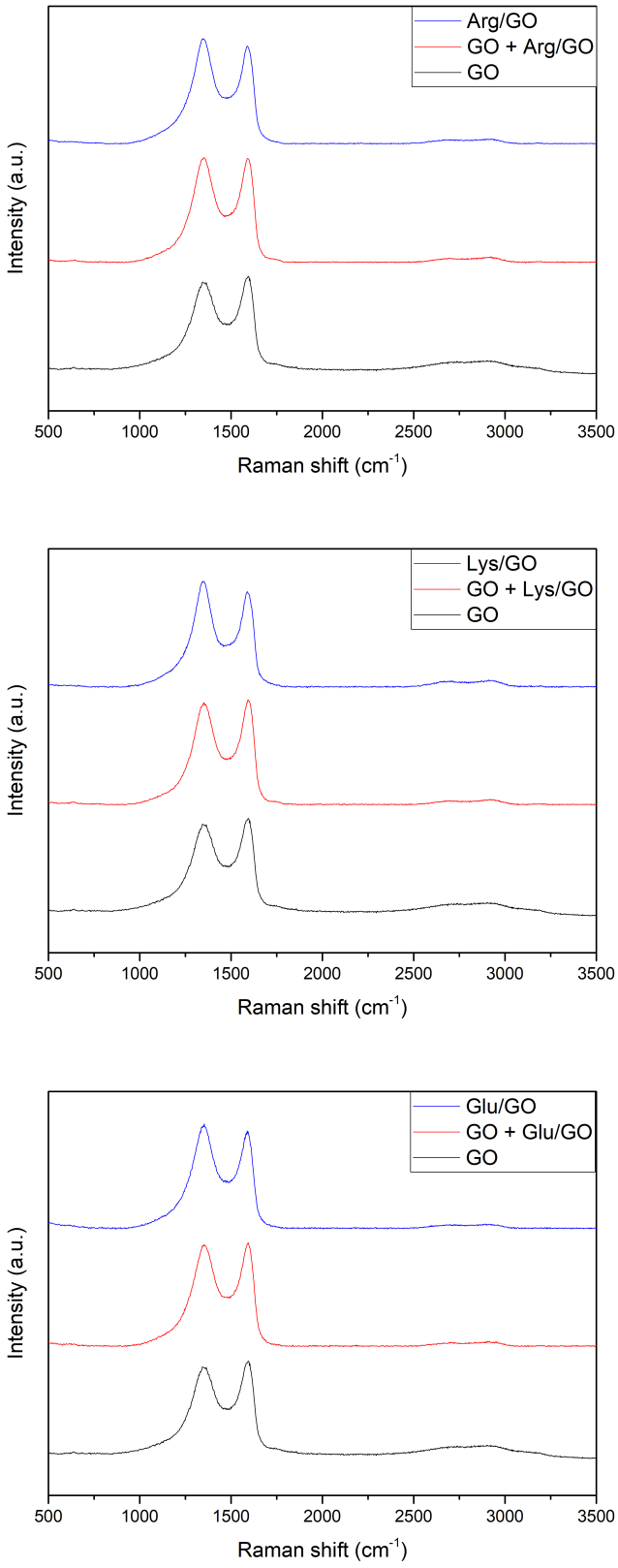


**Figure 4.2:** Comparison of the Raman spectra of GO membranes from ISOF.

Unfortunately, as can be seen in Figure 4.3, an optical microscope does not provide enough magnification to view any interesting features of the GO membranes. Therefore, the results about the morphology of investigated samples are all described in the next section.

**Table 4.1:** Results of the Raman spectroscopy measurements. The 2nd and 3rd columns show the Raman shifts of observed peaks indicating GO. The last columns shows the ratio of the intensity of these 2 peaks for each sample, calculated as the ratio of their areas.

| Sample | D peak position ($cm^{-1}$) | G peak position ($cm^{-1}$) | $I_D/I_G$ |
|---|---|---|---|
| GO | 1350.69 | 1595.66 | 1.22 |
| KGO | 1350.83 | 1599.04 | 2.11 |
| GO (ISOF) | 1351.81 | 1596.46 | 2.31 |
| GO+Arg/GO | 1349.59 | 1596.79 | 2.32 |
| GO+Lys/GO | 1352.31 | 1598.76 | 2.25 |
| GO+Glu/GO | 1353.41 | 1597.20 | 2.39 |
| Arg/GO | 1347.46 | 1595.81 | 2.54 |
| Lys/GO | 1346.81 | 1596.46 | 2.45 |
| Glu/GO | 1349.45 | 1593.63 | 2.72 |

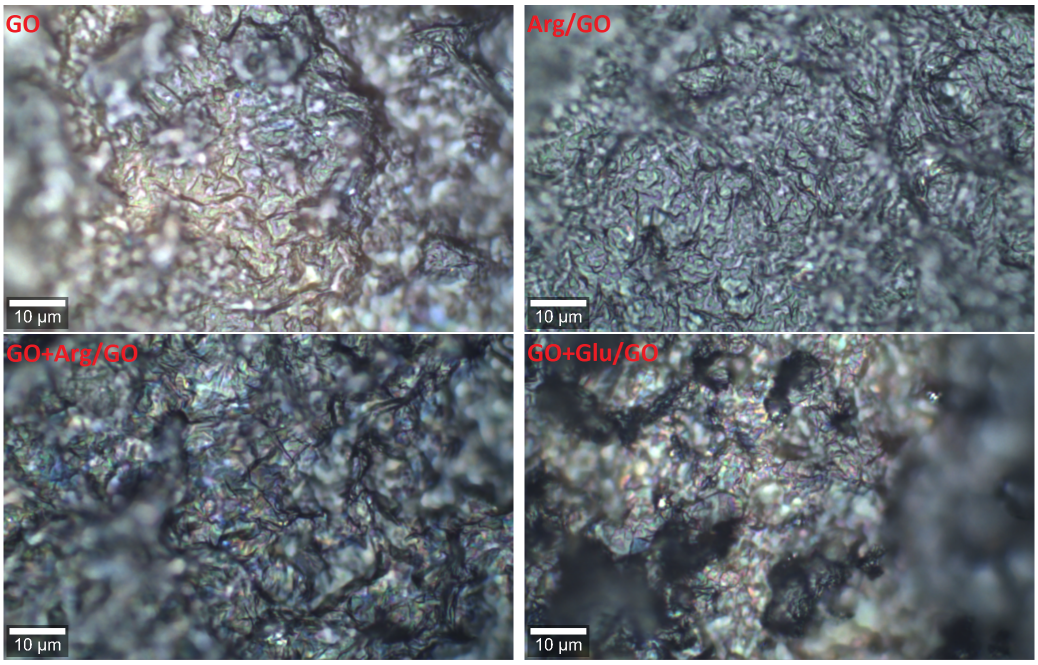


**Figure 4.3:** Pictures taken with an optical microscope included in the WITec alpha300 R setup.

## 4.2 Scanning electron microscopy

As can be clearly seen in Figure 4.4 and 4.5 the synthesised membranes have a thicknesses far below 1 $\mu$m. These figures show cross-sectional SEM images of a

pristine GO membrane as well as potassium-intercalated GO membrane prepared via previously described vacuum filtration method. While the deposited layer of a 2D material is highly wrinkled, following the structure of underlying cellulose acetate substrate, it appears to be covering the substrate quite uniformly, as it covers the entire visible cross-section without any gaps.
However, SEM images taken from above the membrane, depicted in Figure 4.6 reveal a presence of holes throughout a GO membrane, uncovering the underlying substrate. As of right now, it is unclear whether these holes are results of the membrane preparation procedure, or if they appeared later due to the handling of the samples.
The membranes prepared from 1-to-1 mixtures of pristine GO and functionalized GO are presented in Figures 4.7, 4.8, 4.9. This images show both the cross-section, as well as top-side view of the membranes. Once again, the wrinkled structure following the underlying substrate is visible throughout the images. It is worth noting however, that in the case of these samples no holes in the deposited films were observed. Unfortunately, in the case of samples depicted in these figures, the sputtered layer of gold gold got damaged during handling. This led to poorer quality of cross-sectional images.

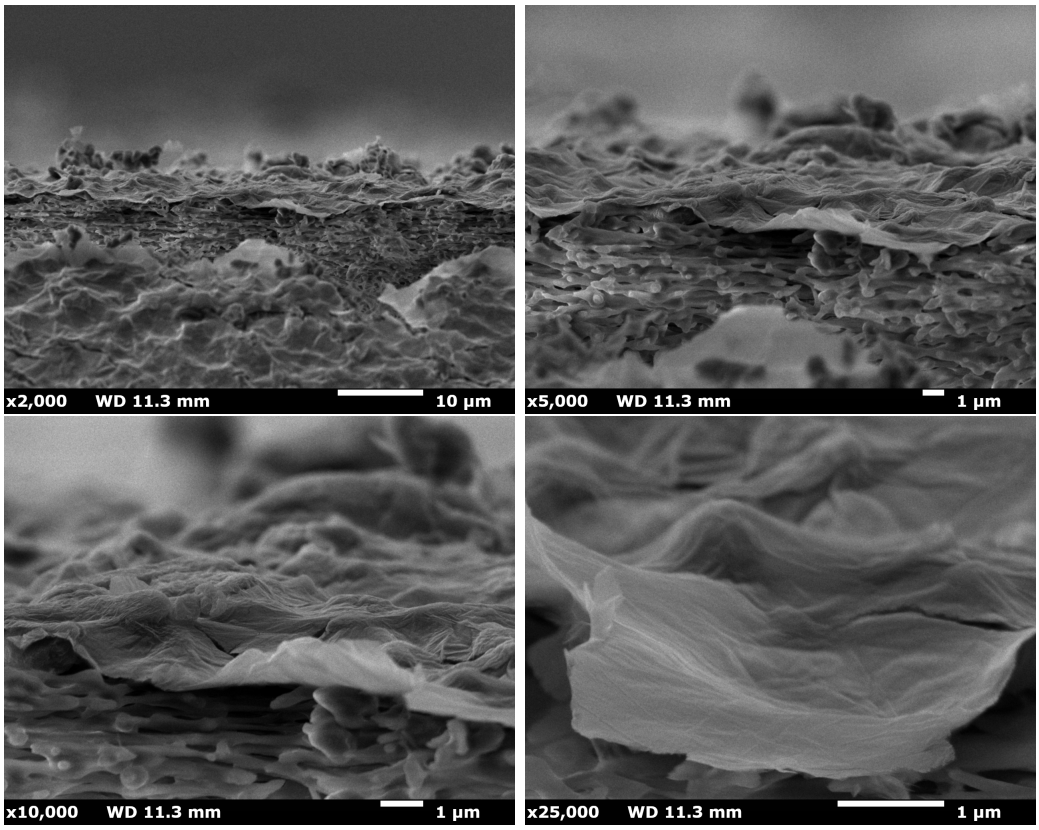


**Figure 4.4:** Cross-sectional SEM images of a 0.2 mg GO membrane without intercalation taken at different magnifications.

Lastly, the SEM images of a GO (ISOF) membrane are shown in Figure 4.10. This figure presents both the top-side view as well as cross-sectional images with increasing magnification. The deposited film appears to be uniformly covering the

underlying substrate. Much like in the case of the functionalized membranes, no holes were observed in this sample.

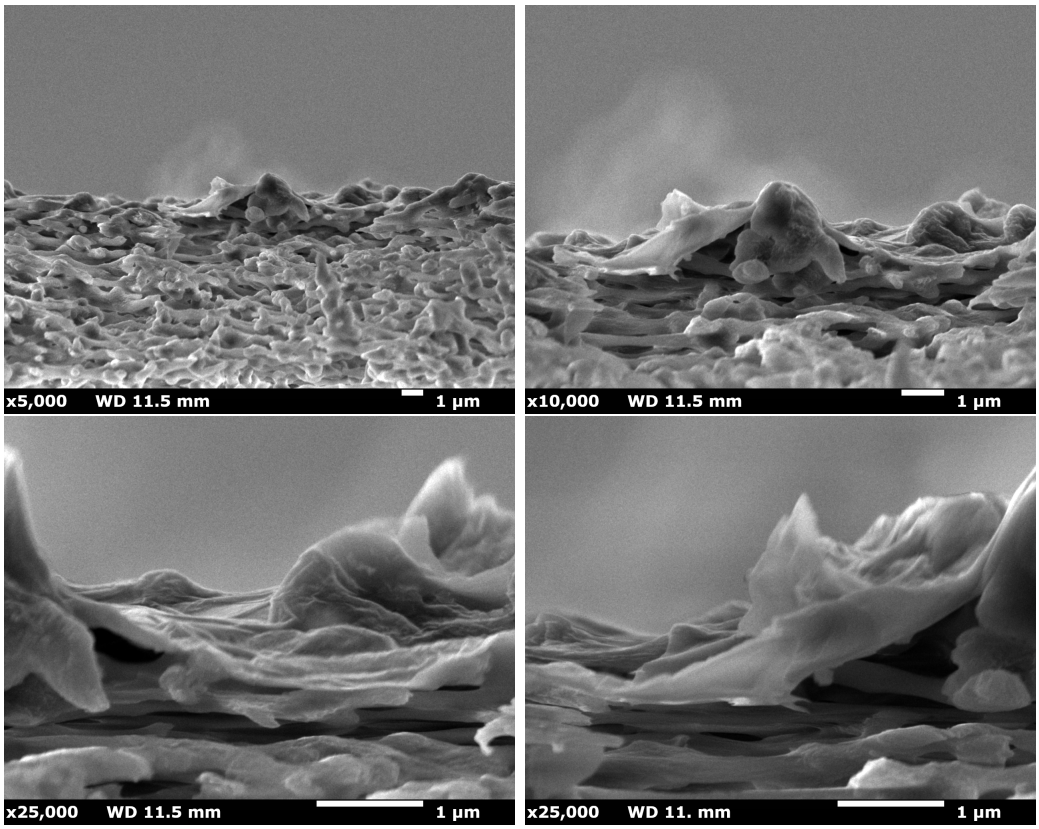


**Figure 4.5:** Cross-sectional SEM images of a 0.2 mg GO membrane intercalated with potassium (KGO) taken at different magnifications.

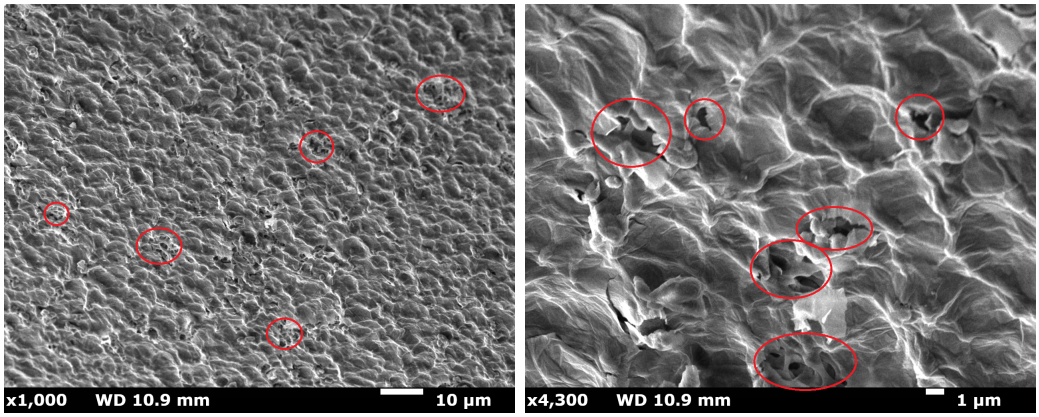


**Figure 4.6:** Examples of the holes. circled in red, visible on some of the GO membranes.

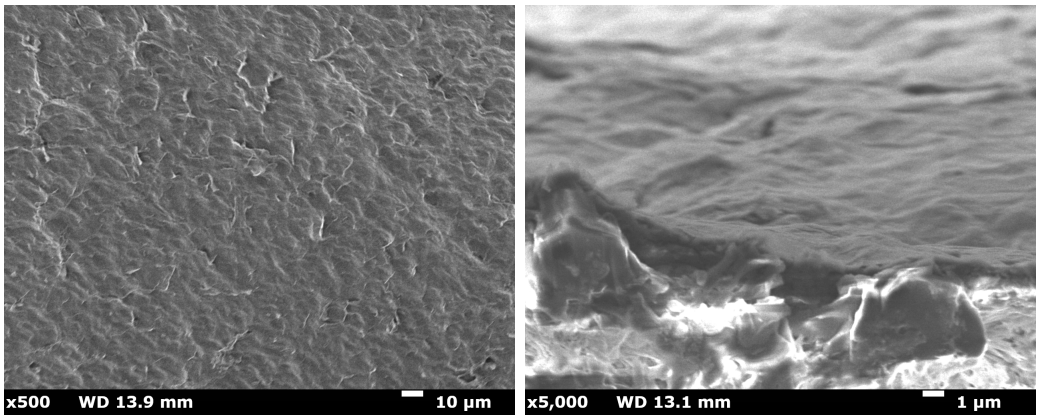


**Figure 4.7:** SEM images showing morphology of the GO membrane prepared from a 1-to-1 mixture of pure GO and Arganine functionalized GO (GO+Arg/GO).

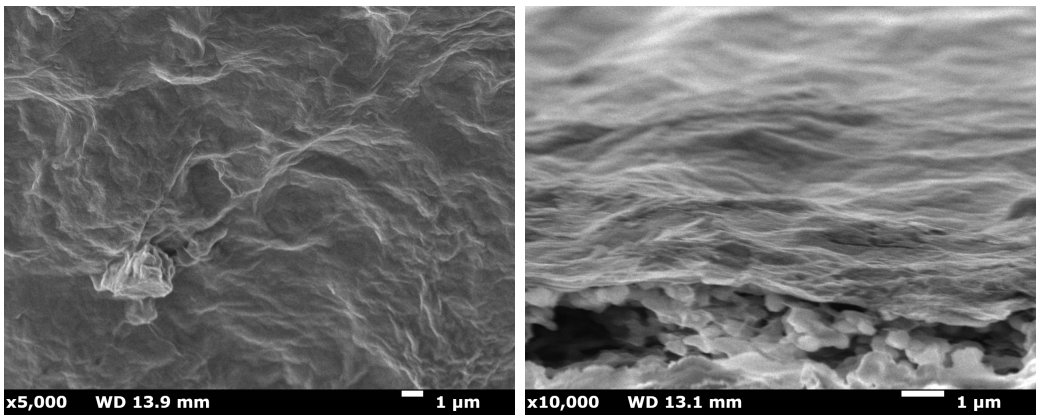


**Figure 4.8:** SEM images showing morphology of the GO membrane prepared from a 1-to-1 mixture of pure GO and Lysine functionalized GO (GO+Lys/GO).

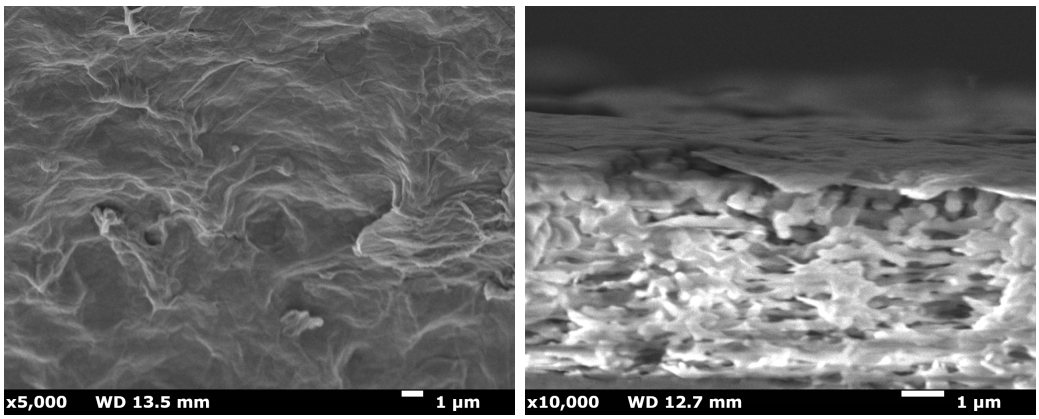


**Figure 4.9:** SEM images showing morphology of the GO membrane prepared from a 1-to-1 mixture of pure GO and Glutamate functionalized GO (GO+Glu/GO).

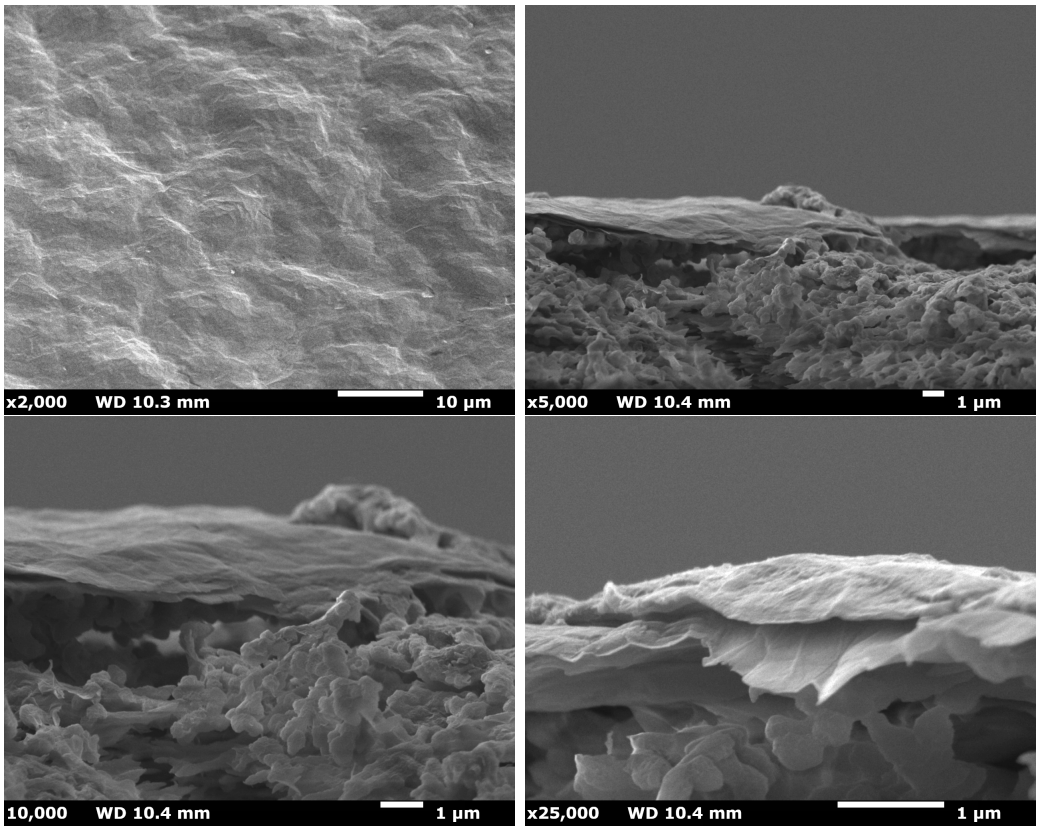


**Figure 4.10:** SEM images showing morphology of the GO membrane from ISOF without functionalization.

## 4.3 X-ray diffraction

As was explained in the section 3.2.3., the XRD measurements provide information about how different modifications of the GO membranes affect their interlayer spacing and swelling properties.

Firstly, a freestanding GO membrane was measured using XRD. the obtained spectrum is presented in Figure 4.11. The $2\,\Theta$ value of the visible peak was determined to be 11.4 degrees, which corresponds to an interlayer spacing of $0,78$ nm. The obtained value is in agreement with that reported in literature [5]. This indicates that the GO powder used for the purpose of this thesis is compatible with those used in other similar works in this area.

In the figures presented in this section, "Dry" spectra indicate that the measured membrane was placed in the spectrometer without any further modifications, "Wet" designates samples which were submerged under water for half an hour before the measurements and "K" indicates that samples were submerged in a 1.5 M solution of KCl prior to XRD measurements.

Ideally, the same membranes as those used for permeation tests would be also measured with XRD. Unfortunately, a membrane with a loading of 0.2 mg of GO is too thin to be investigated using this method. Therefore, a thicker membrane, as explained in the section 3.1, was utilized to evaluate the effects of potassium inter-

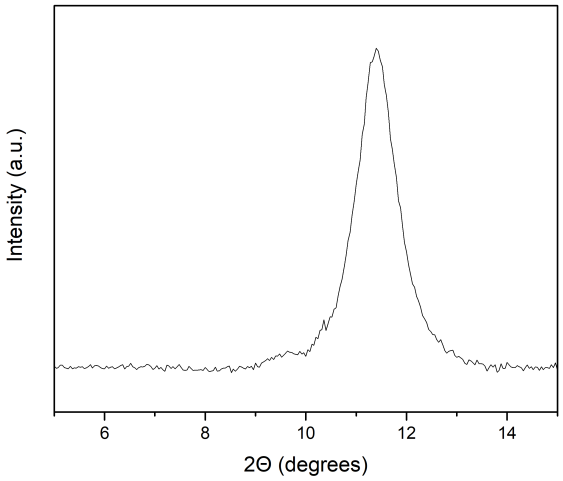


**Figure 4.11:** XRD spectrum of a freestanding GO membrane.

calation. The results of this measurements are presented in Figure 4.12. This data clearly confirms that there is a large increase in interlayer spacing upon wetting in water (shift towards smaller angles). Moreover, it can be seen that this shift is slightly reduced when the potassium ions are intercalated into the GO membrane.

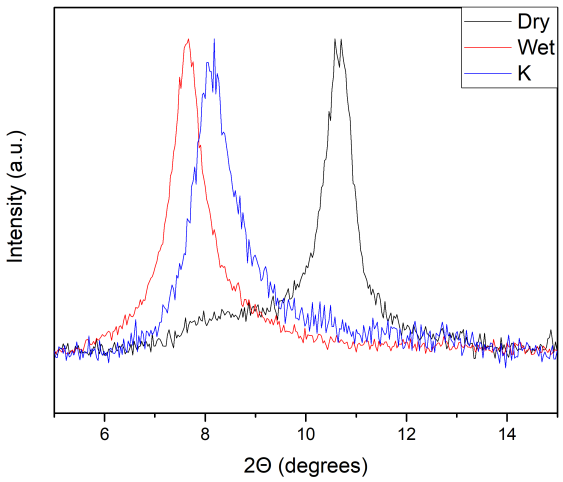


**Figure 4.12:** XRD spectra of a GO membrane supported with cellulose acetate.

The effects of three different functional species (Arg, Lys and Glu) are presented in Figure 4.13. Since these membranes were prepared using a different GO powder as well as different cellulose acetate membrane, a pure GO membrane made up of the same ingredients was also measured as a reference, with resulting spectra presented in Figure 4.13. In this sample, the shift from wetting is far less pronounced. This seems to suggest that the covalent functionalization is more suited for the prevention of swelling. Notably, membranes which were intercalated with potassium on top of

being functionalized shown larger increase in the interlayer spacing. Interestingly, pure GO membrane from ISOF exhibits the same behaviour as the functionalized samples, therefore, the reluctance to swelling observed in pure GO membrane in this paragraph might actually come from the slight reduction of GO which they were subjected to. This would also explain why the intercalation with potassium caused them to loose their anti-swelling property. Reduced graphene oxide under normal conditions is hydrophobic, which is why it does not readily swell in water. However, potassium ions introduce additional charge on the surface of its layers, which can make it hydrophilic again.
The interlayer distances calculated from positions of peaks present in the data depicted above are shown in Table 4.2. For additional clarity, the same values are also presented in Figure 4.14.

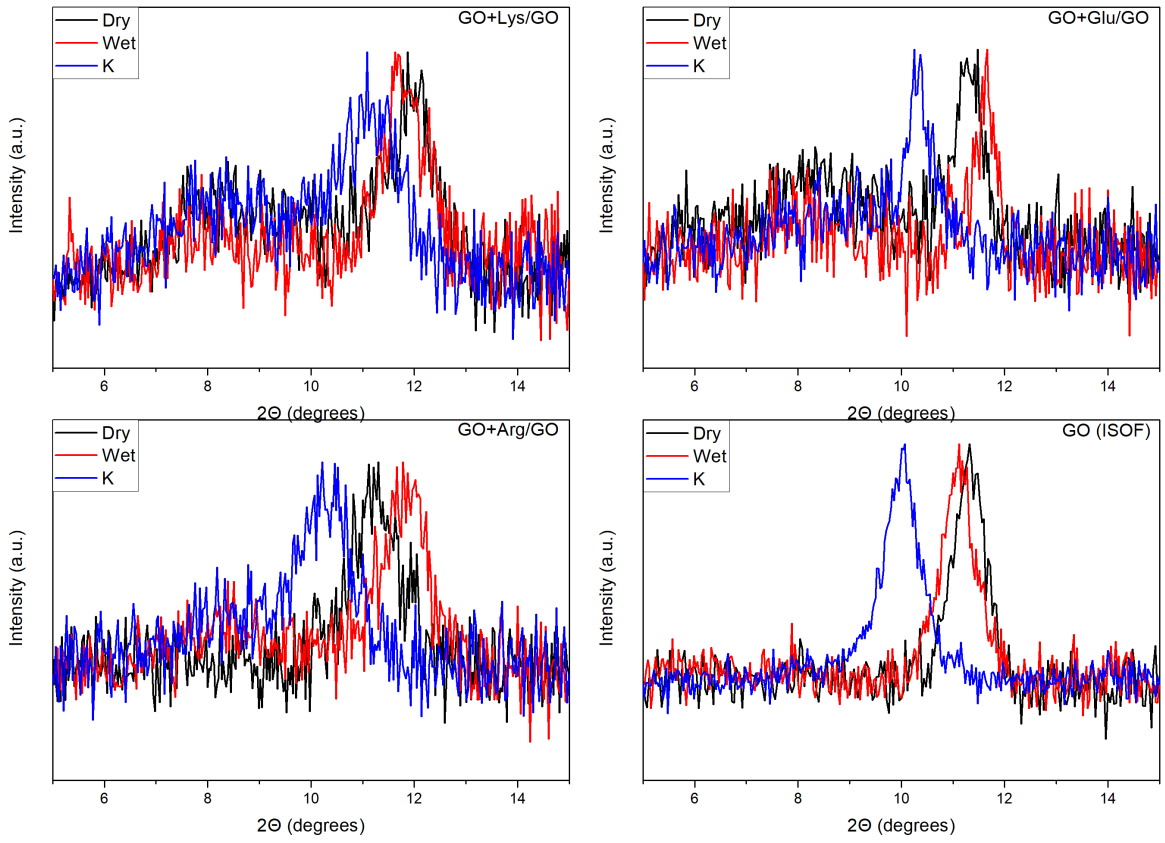


**Figure 4.13:** XRD spectra of the GO+Arg/GO, GO+Lys/GO, GO+Glu/GO and GO (ISOF) membranes.

In order to better understand changes which might occur in a membrane after ion permeation, XRD spectra of dry and wetted membranes previously used for the permeation of iron were recorded. These spectra are presented in Figure 4.15. Unfortu-

**Table 4.2:** Interlayer distances calculated from the XRD data of the investigated membranes.

| Membrane type | "Dry" distance(nm) | "Wet" distance(nm) | "K" distance(nm) |
|---|---|---|---|
| GO | 0.83 | 1.15 | 1.08 |
| Arg+GO | 0.79 | 0.75 | 0.87 |
| Lys+GO | 0.74 | 0.75 | 0.79 |
| Glu+GO | 0.78 | 0.76 | 0.86 |
| GO-ISOF | 0.78 | 0.80 | 0.88 |

nately, the pure GO membrane from ISOF did not show any clear peak in its XRD spectra after ion permeation. As for the other three samples, both GO+Lys/GO and GO+Glu/GO behaved in the same manner as they did before ion permeation, showing very little shift, if any, upon the wetting. GO+Arg/GO membrane however noticeably expended after being submerged in water. This shift appears to be analogous to the one visible in Figure 4.12, making it seem as though the $Fe^{3+}$ ions displaced Arg functional groups.

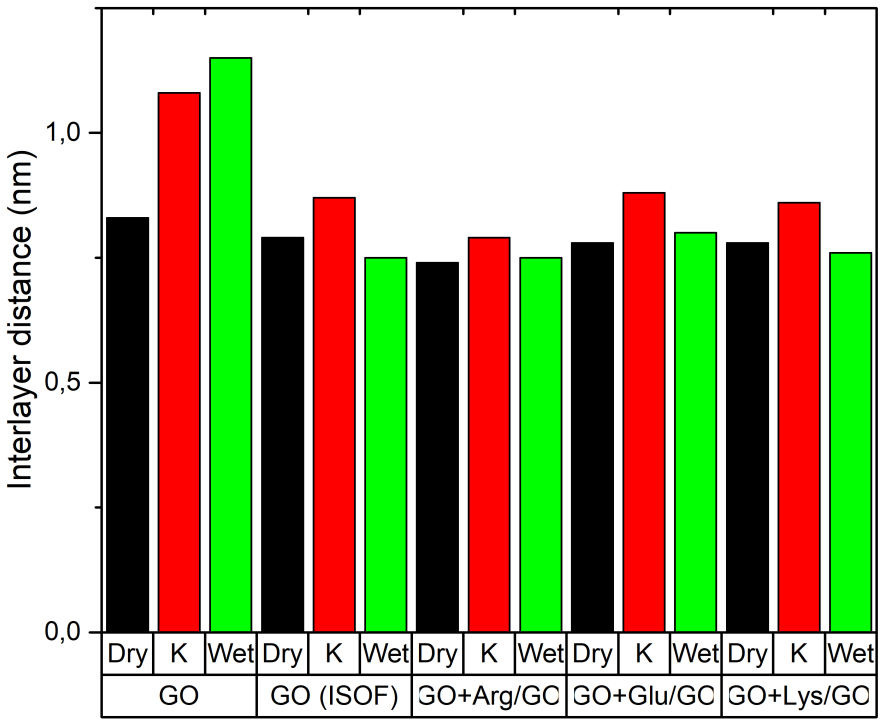


**Figure 4.14:** Interlayer distances calculated from the XRD data of the investigated membranes.

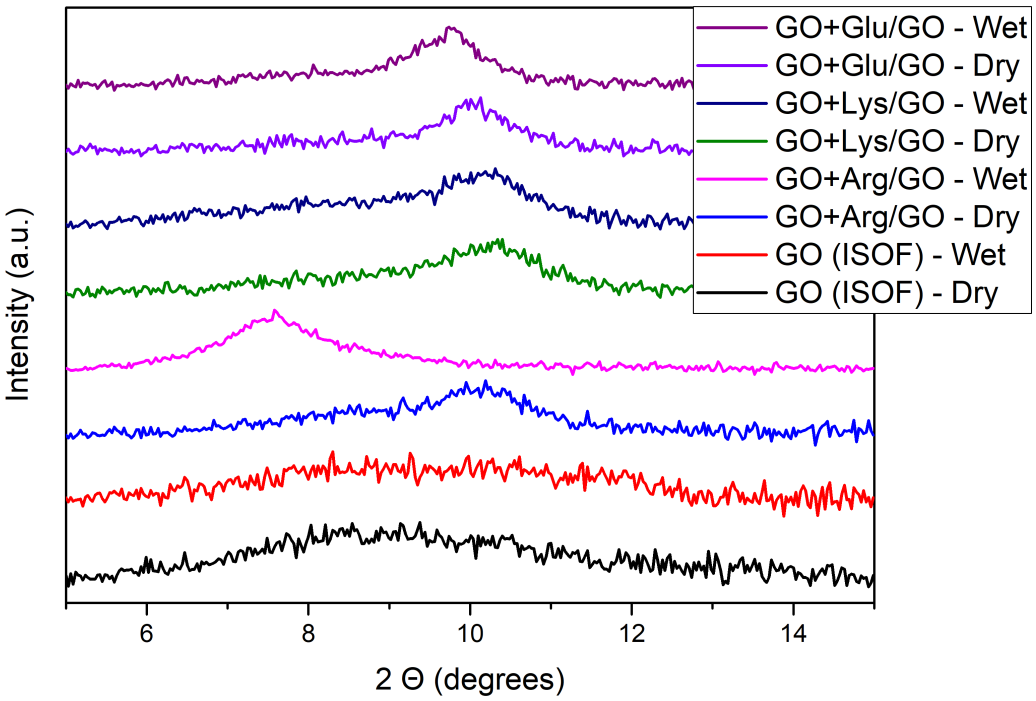


**Figure 4.15:** XRD spectra of the functionalized and pristine GO membranes from ISOF after iron permeation tests.

## 4.4 Permeation tests

As was explained in the methods section, the ability of a given membrane to selectively block ionic species was evaluated based on the changes of conductance over time in the experimental setup depicted in Figure 3.3. The data presented in Figure 4.16 shows typical dependence of conductance on the permeation time. This particular curve was obtained for a potassium intercalated GO membrane during lithium and iron permeation tests. For the rest of this section, this curves will serve as examples to give the reader a better understanding of the way in which the permeation rates and selectivities were calculated from the changes in conductance.

Figure 4.17 show the calibration curves prepared in order to establish precise connection between conductance and concentration. LiCl shows a linear relationship between conductance and concentration throughout the entire range of measurements. However, the same cannot be said for $FeCl_3$, which is typical of stronger electrolytes such as this. Which is why, the standard procedure for calculating concentration from the measured conductance is to prepare different linear approximations for different ranges of conductance value. An example of such approach can be seen in Table 4.3. It shows conversion factors which can be used to calculate the total dissolved solids.

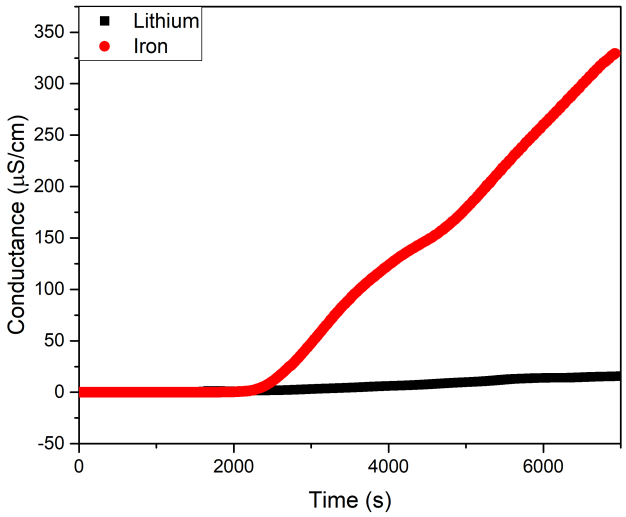


**Figure 4.16:** Example of the conductance curves obtained during permeation tests.

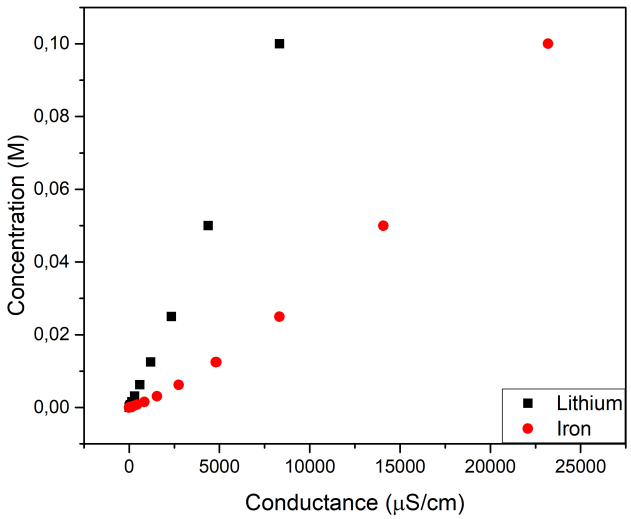


**Figure 4.17:** Calibration data obtained for LiCl and $FeCl_3$ solutions.

**Table 4.3:** Conversion factors used to calculate the total dissolved solids from conductance. This data was taken from the manual to the multiparameter used in this thesis.

| Conductance | Conversion factor |
|---|---|
| 1-100 $\mu$S/cm | 0.60 |
| 100-1000 $\mu$S/cm | 0.71 |
| 1-10 mS/cm | 0.81 |
| 10-200 mS/cm | 0.94 |

As can be clearly seen in Figure 4.16, in both cases (lithium permeation and iron permeation) it takes between half an hour to an hour for the permeation to begin. Afterwards the conductance grows in a uniform manner. Therefore, only the values measured during the last hour of an experiment were used in order to calculate the permeation rate for a given sample. In the case of the data presented in Figure 4.16 this time period corresponds to the conductance in the range from 4 to 16 $\mu$S/cm for lithium and from 80 to 330 $\mu$S/cm for iron. The data from calibration curves restricted to these regions, together with fitted linear approximations, are presented in Figure 4.18. These fitted linear functions were then in turn used to calculate the values for concentrations in the last hour of permeation experiments. The results of this calculations are depicted in Figure 4.19. The permeation rates were calculated from the slopes of linear functions fitted to the concentration vs time plots according to equation 3.2. The effective area of the membrane (area of the part in contact with the solutions), needed for this equation, in the case of this experimental setup, was equal to $\sim$1.77 cm$^2$. All of the permeation rates calculated in this manner are presented in Table 4.4. Table 4.5 shows the selectivities calculted from the permeation rates.

**Table 4.4:** Permeation rates calculated from the measurements of changes in conductance over time.

| Membrane type | Lithium permeation rate (mol/(m$^2$h)) | Iron permeation rate (mol/(m$^2$h)) |
|---|---|---|
| GO | 0.0094 | 0.0654 |
| KGO | 0.0225 | 0.0817 |
| GO (ISOF) | 0.0014 | 0.0486 |
| GO+Arg/GO | 0.0064 | 0.0003 |
| GO+Lys/GO | 0.0004 | 0.0001 |
| GO+Glu/GO | 0.0002 | 0.0285 |

**Table 4.5:** Ionic selectivities calculated from previously obtained permeation rates

| Membrane type | Selectivity |
|---|---|
| GO | 0.14 |
| KGO | 0.28 |
| GO (ISOF) | 0.05 |
| GO+Arg/GO | 20.13 |
| GO+Lys/GO | 2.84 |
| GO+Glu/GO | 0.14 |

For additional clarity, the calculated permeation rates and selectivities are also presented in Figure 4.20. Out of the three membranes utilizing covalent functionalization, the one decorated with Glu appears to have its properties closest to pristine GO membrane. This is attributed to the fact that a Glu molecule is terminated by a carboxyl groups on both sides. This group is already present on the GO sheets. Arg and Lys on the other hand are both terminated with amine groups on one of their

sides. These groups can become protonated in water, introducing positive surface charge, which is not present in neither pristine nor Glu decorated GO.
Interestingly, for majority of the investigated membranes, the $Li^+$ ions appear to be penetrating slower than the $Fe^{3+}$ ions, indicated by a value for selectivity being lower than 1. It is contradictory to the commonly accepted theory that size exclusion is the main mechanism responsible for selectivity of 2D membranes, as was explained in the section 2.3. This result is also in stark contrast to similar tests performed on GO-based membranes reported in literature [3].
A possible explanation to this inconsistency is the method selected in this thesis for measuring concentration. Even when $Fe^{3+}$ ions are blocked by the membrane, it is still possible for that the counterions, namely $Cl^-$, can penetrate it. Naturally, an increase of anion concentration would need to be compensated for. Therefore, hydrogen $H^+$ ions would have to travel through the membrane together with $Cl^-$ ions. This change to the ionic composition would lead to an increase of a measured conductance, event without an increase of the concentration of the cations of interest. However, in order to evaluate this hypothesis, further experiments are needed.
One possible way of investigating this issue further is to utilize pH measurements. As explained in the previous paragraph, the $Cl^-$ ions travelling through the membrane would have to be accompanied by $H^+$. Therefore, they would cause the DI water side of the permeation setup to become more acidic. As such, pH measurements could be used as a proof of the proposed expalnation.
Additionally, utilizing another, more reliable, method of measuring concentrations as a reference is another possible approach. To that end, Inductively Coupled Plasma Atomic Emission Spectroscopy (ICP-OES) would be the preferred choice, as it is often used in this types of experiments [3]. With this in mind, solutions before and after permeation tests were collected during the experiments, making it possible to use them for the ICP-OES measurements.
Unfortunately, the time-frames for the thesis, did not allow for either of the above mentioned refinements to the measuring procedure. Therefore, this work remains to be done in the future.

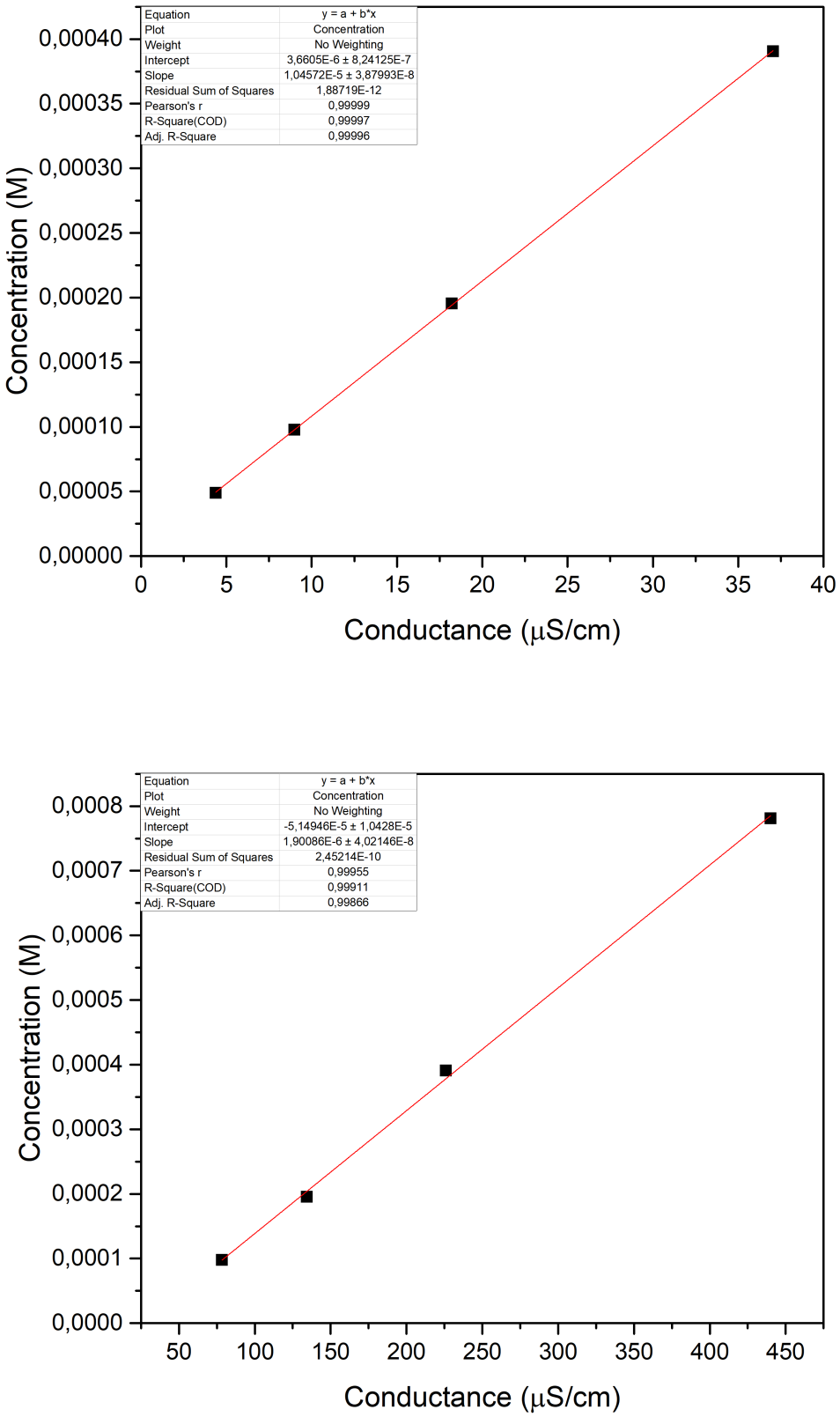


**Figure 4.18:** Calibration curves obtained for LiCl (top) and $FeCl_3$ (bottom) restricted to the relevant ranges of conductance together with fitted linear functions.

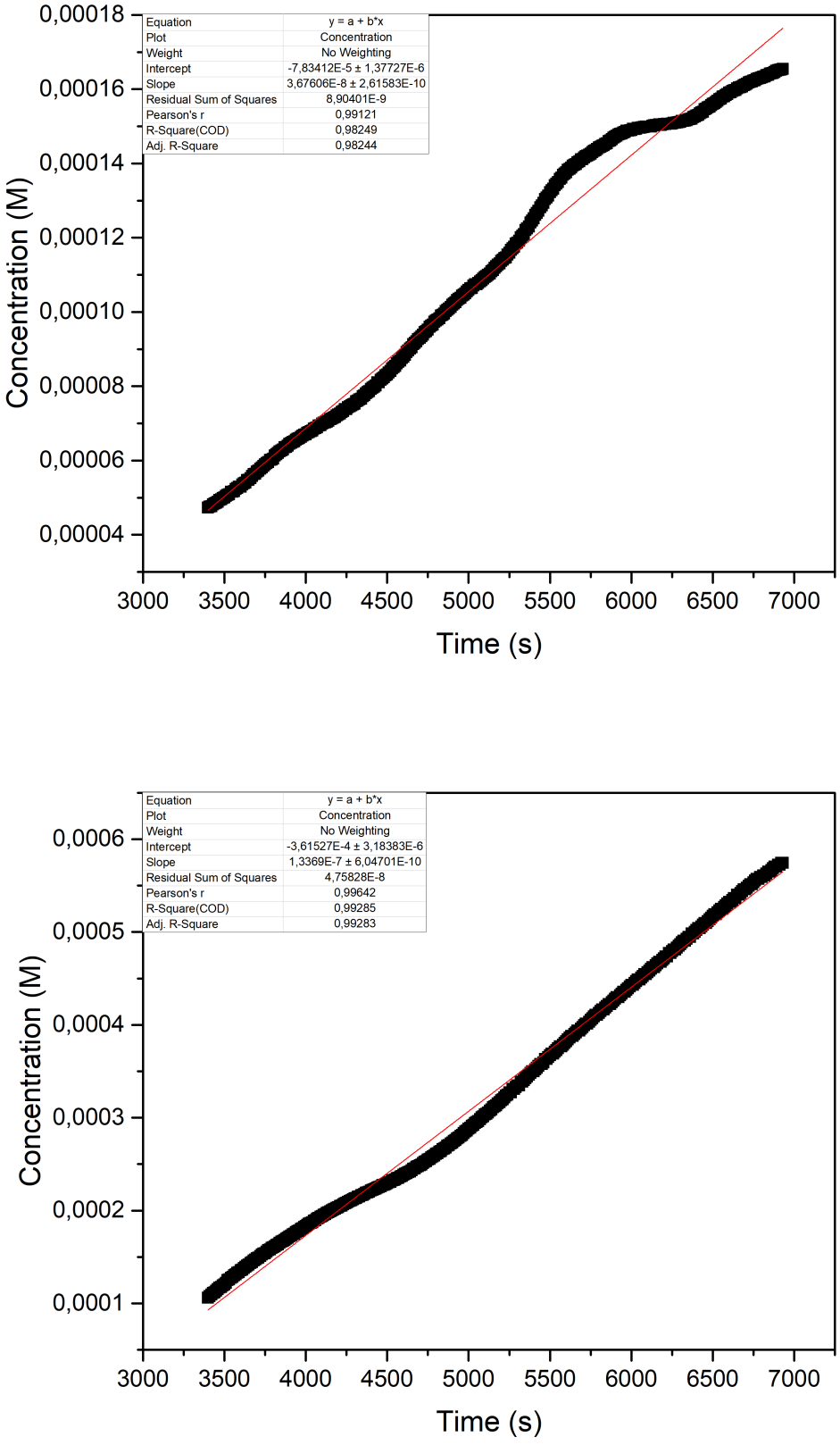


**Figure 4.19:** Concentrations of LiCl (top) and $FeCl_3$ (bottom) over time calculated for the last hour of their respective permeation experiments together with fitted linear functions.

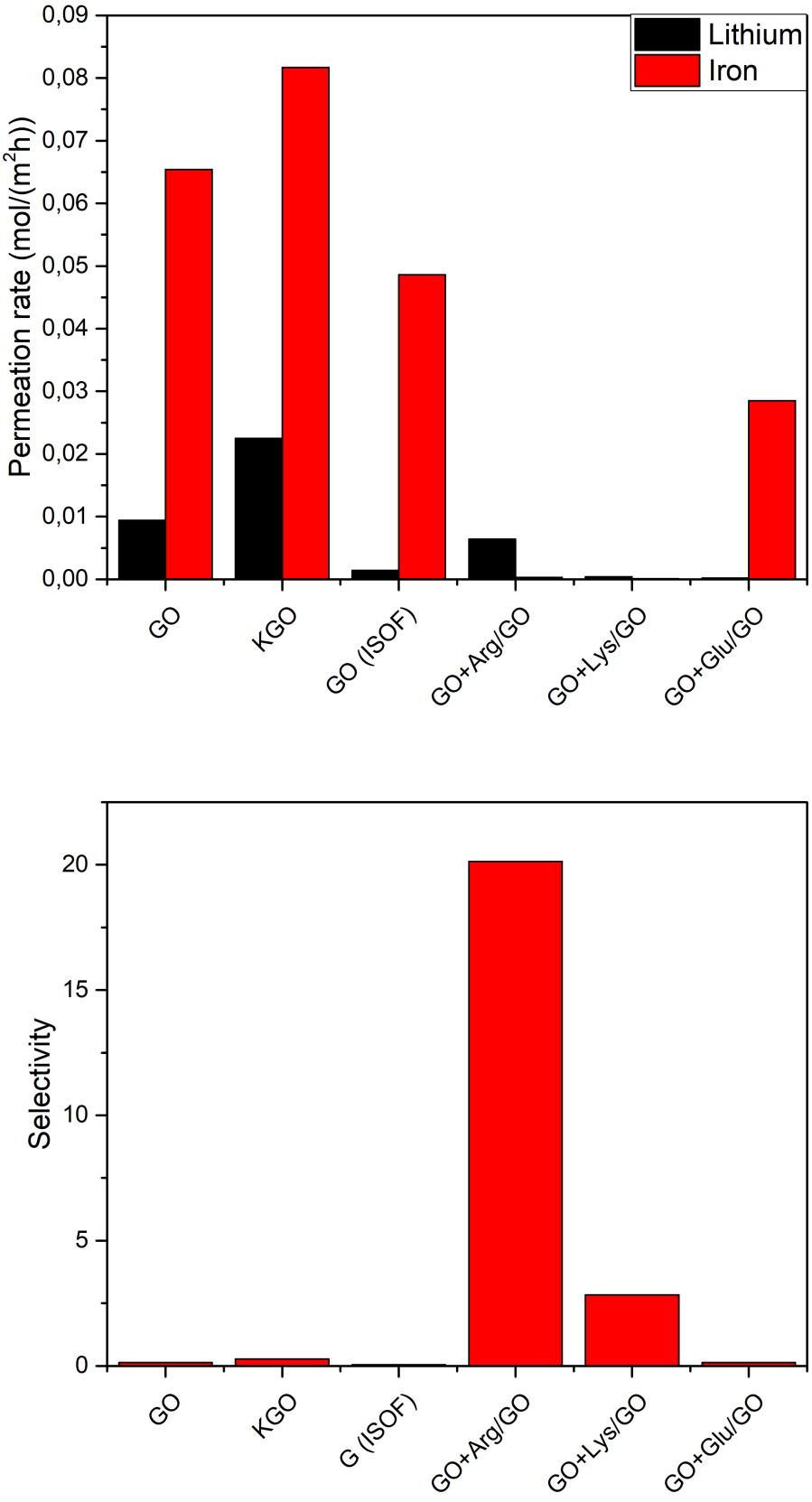


**Figure 4.20:** Permeation rates (top) and selectivities (bottom) calculated from the measurements of changes in conductance over time.

# 5

# Conclusion and future prospects

The original purpose of this Master's thesis was twofold. Firstly, various approaches to the tuning of the interlayer spacing and prevention of swelling in water of GO-based membranes were to be investigated and compared between one another. Secondly, the capability of the aforementioned membranes to be used in ion separation application (specifically lithium extraction) was to be evaluated.
In the end, 4 different methods of modifying GO membranes were compared with each other. These include potassium ion intercalation as well as functionalization with arginine, lysine and glutamate. Their effects on the interlayer spacing and stability of GO membranes was best visible in the results from XRD measurements. According to these results, all three covalent functionalization methods appear to be better suited for the purpose of swelling prevention than the potassium intercalation. Although, further inquiries, that decorating GO layers with Lys and Glu is a more durable approach, as their behaviour did not change after iron permeation tests, unlike the one observed for Arg-modified sample.
As for the selectivity of investigated membranes, here the results are much less clear. Majority of the tested membranes showed higher permeation rates for iron, instead of lithium, which was a direct opposite to what was initially expected based on the theoretical considerations as well as similar tests reported in literature [3]. Only the membranes modified with Arg and Lys showed the expected tendency to block out iron cations while allowing lithium cations to pass through.
This unexpected result might have been caused by the selected method of measuring ionic concentration. It is possible that the counterions originating from the salt ($Cl^-$), could penetrate the membrane faster than the cations of interest, disturbing the relation between conductance and cation concentration obtained from the prepared calibration curves.
In light of the above consideration, any further works on this topic should start by verifying the method of measuring concentrations utilized for the purpose of this Master's thesis. This could be done in one or both of the following approaches. Firstly, any changes in the stoichiometric ratio of cations to anions of a dissolved salt should in turn affect the concentration of hydrogen ions in the solution. Therefore, pH measurements could be used to validate the hypothesis presented in the previous paragraph. Secondly, a more reliable method of measuring concentration, such as ICP-OES, could be used as a reference to validate or invalidate results obtained in this thesis.

# Bibliography


[1] K. S. Novoselov *et al.*, "Electric field effect in atomically thin carbon films," *science*, vol. 306, no. 5696, pp. 666–669, 2004.

[2] V. Shanmugam *et al.*, "A review of the synthesis, properties, and applications of 2d materials," *Particle & Particle Systems Characterization*, vol. 39, no. 6, p. 2 200 031, 2022.

[3] S. Wang, Y. Yang, J. Liu, L. Chen, S. Liang, and H. Fang, "Unexpected ion sieving in graphene oxide membranes," *The Journal of Physical Chemistry C*, vol. 126, no. 22, pp. 9572–9579, 2022.

[4] Z. Wang *et al.*, "Ion sieving in graphene oxide membrane enables efficient actinides/lanthanides separation," *Nature Communications*, vol. 14, no. 1, p. 261, 2023.

[5] L. Chen *et al.*, "Ion sieving in graphene oxide membranes via cationic control of interlayer spacing," *Nature*, vol. 550, no. 7676, pp. 380–383, 2017.

[6] P. Jia *et al.*, "The combination of 2d layered graphene oxide and 3d porous cellulose heterogeneous membranes for nanofluidic osmotic power generation," *Molecules*, vol. 26, no. 17, p. 5343, 2021.

[7] A. G. Fane, R. Wang, and M. X. Hu, "Synthetic membranes for water purification: Status and future," *Angewandte Chemie International Edition*, vol. 54, no. 11, pp. 3368–3386, 2015.

[8] T. Foller, H. Wang, and R. Joshi, "Rise of 2d materials-based membranes for desalination," *Desalination*, vol. 536, p. 115 851, 2022.

[9] T. Zhao *et al.*, "A review on the recycling of spent lithium iron phosphate batteries," *Journal of Environmental Management*, vol. 351, p. 119 670, 2024.

[10] Y. Yang *et al.*, "A closed-loop process for selective metal recovery from spent lithium iron phosphate batteries through mechanochemical activation," *ACS Sustainable Chemistry & Engineering*, vol. 5, no. 11, pp. 9972–9980, 2017.

[11] M. Wang *et al.*, "Recycling of lithium iron phosphate batteries: Status, technologies, challenges, and prospects," *Renewable and Sustainable Energy Reviews*, vol. 163, p. 112 515, 2022.

[12] M. Anton, *The relation of graphene to graphite.* Wikimedia Commons. `https://pl.wikipedia.org/wiki/Plik:Graphene-graphite_relation.png`, 2009.

[13] D. R. Cooper *et al.*, "Experimental review of graphene," *International Scholarly Research Notices*, vol. 2012, 2012.

[14] A. Dabrowska, M. K. Kurcz, and A. Huczko, *Grafen: otrzymywanie, charakterystyka, zastosowania.* Wydawnictwa Uniwersytetu Warszawskiego, 2018.

[15] Ponor, *Sigma and pi bonds in graphene. sigma bonds result from an overlap of sp2 hybrid orbitals, whereas pi bonds emerge from tunneling between the protruding pz orbitals. for clarity, only a few neighboring pz orbitals are shown*, Wikimedia Commons. https://commons.wikimedia.org/wiki/File:Graphene_-_sigma_and_pi_bonds.svg, 2020.

[16] W. Yu, L. Sisi, Y. Haiyan, and L. Jie, "Progress in the functional modification of graphene/graphene oxide: A review," *RSC advances*, vol. 10, no. 26, pp. 15 328–15 345, 2020.

[17] Iridos, *Graphene oxide. see papers.* Wikimedia Commons. https://commons.wikimedia.org/wiki/File:Graphite_oxide.svg, 2012.

[18] E. Jaafar, M. Kashif, S. K. Sahari, and Z. Ngaini, "Study on morphological, optical and electrical properties of graphene oxide (go) and reduced graphene oxide (rgo)," in *Materials Science Forum*, Trans Tech Publ, vol. 917, 2018, pp. 112–116.

[19] J. W. Suk, R. D. Piner, J. An, and R. S. Ruoff, "Mechanical properties of monolayer graphene oxide," *ACS nano*, vol. 4, no. 11, pp. 6557–6564, 2010.

[20] L. Liu, J. Zhang, J. Zhao, and F. Liu, "Mechanical properties of graphene oxides," *Nanoscale*, vol. 4, no. 19, pp. 5910–5916, 2012.

[21] S. Zhang, H. Wang, J. Liu, and C. Bao, "Measuring the specific surface area of monolayer graphene oxide in water," *Materials Letters*, vol. 261, p. 127 098, 2020.

[22] Z.-S. Wu, W. Ren, L. Gao, B. Liu, C. Jiang, and H.-M. Cheng, "Synthesis of high-quality graphene with a pre-determined number of layers," *Carbon*, vol. 47, no. 2, pp. 493–499, 2009.

[23] A. Jiříčková, O. Jankovskỳ, Z. Sofer, and D. Sedmidubskỳ, "Synthesis and applications of graphene oxide," *Materials*, vol. 15, no. 3, p. 920, 2022.

[24] W. Yu, L. Sisi, Y. Haiyan, and L. Jie, "Progress in the functional modification of graphene/graphene oxide: A review," *RSC advances*, vol. 10, no. 26, pp. 15 328–15 345, 2020.

[25] J. W. M. et al. "11.4: Hydration of ions - chemistry libretexts." (), [Online]. Available: https://chem.libretexts.org/Bookshelves/General_Chemistry/ChemPRIME_(Moore_et_al.)/11%3A_Reactions_in_Aqueous_Solutions/11.04%3A_Hydration_of_Ions (visited on 05/25/2024).

[26] E. Nightingale Jr, "Phenomenological theory of ion solvation. effective radii of hydrated ions," *The Journal of Physical Chemistry*, vol. 63, no. 9, pp. 1381–1387, 1959.

[27] L. Ding *et al.*, "Effective ion sieving with ti3c2t x mxene membranes for production of drinking water from seawater," *Nature Sustainability*, vol. 3, no. 4, pp. 296–302, 2020.

[28] J. Abraham *et al.*, "Tunable sieving of ions using graphene oxide membranes," *Nature nanotechnology*, vol. 12, no. 6, pp. 546–550, 2017.

[29] J. Ran *et al.*, "Non-covalent cross-linking to boost the stability and permeability of graphene-oxide-based membranes," *Journal of materials chemistry A*, vol. 7, no. 14, pp. 8085–8091, 2019.

[30] M. Tagliazucchi and I. Szleifer, "Transport mechanisms in nanopores and nanochannels: Can we mimic nature?" *Materials Today*, vol. 18, no. 3, pp. 131–142, 2015.

[31] M.-L. Bocquet, *Snapshot of graphene oxide in liquid water from molecular dynamics simulation*, Wikimedia Commons. `https://commons.wikimedia.org/wiki/File:Graphene_oxide_in_liquid_water.png`, 2020.

[32] A. Iakunkov and A. V. Talyzin, "Swelling properties of graphite oxides and graphene oxide multilayered materials," *Nanoscale*, vol. 12, no. 41, pp. 21 060–21 093, 2020.

[33] G. Yuan *et al.*, "Ion and molecule sieving through highly stable graphene-based laminar membranes," *The Journal of Physical Chemistry Letters*, vol. 14, no. 7, pp. 1702–1707, 2023.

[34] A. S. Mahadevi and G. N. Sastry, "Cation- $\pi$ interaction: Its role and relevance in chemistry, biology, and material science," *Chemical reviews*, vol. 113, no. 3, pp. 2100–2138, 2013.

[35] P. M. V. Raja and A. R. Barron. "4.3: Raman spectroscopy - chemistry libretexts." (), [Online]. Available: `https://chem.libretexts.org/Bookshelves/Analytical_Chemistry/Physical_Methods_in_Chemistry_and_Nano_Science_(Barron)/04%3A_Chemical_Speciation/4.03%3A_Raman_Spectroscopy` (visited on 05/25/2024).

[36] K. D. Vernon-Parry, "Scanning electron microscopy: An introduction," *III-Vs review*, vol. 13, no. 4, pp. 40–44, 2000.

[37] G. F. Harrington and J. Santiso, "Back-to-basics tutorial: X-ray diffraction of thin films," *Journal of Electroceramics*, vol. 47, no. 4, pp. 141–163, 2021.

[38] A. S. Khune *et al.*, "Highly sensitive, selective, repeatable and flexible chemiresistive no2 sensor based on reduced graphene oxide/free based porphyrin composite," *Journal of Materials Science: Materials in Electronics*, vol. 35, no. 9, p. 672, 2024.

[39] F. T. Johra, J.-W. Lee, and W.-G. Jung, "Facile and safe graphene preparation on solution based platform," *Journal of Industrial and Engineering Chemistry*, vol. 20, no. 5, pp. 2883–2887, 2014.

[40] H. Y. Mohammed, M. A. Farea, Z. M. Ali, S. M. Shirsat, M.-L. Tsai, and M. D. Shirsat, "Poly (n-methyl pyrrole) decorated rgo nanocomposite: A novel ultrasensitive and selective carbon monoxide sensor," *Chemical Engineering Journal*, vol. 441, p. 136 010, 2022.

[41] S. Stankovich *et al.*, "Synthesis of graphene-based nanosheets via chemical reduction of exfoliated graphite oxide," *carbon*, vol. 45, no. 7, pp. 1558–1565, 2007.

[42] M. Baraket, S. Walton, Z. Wei, E. Lock, J. Robinson, and P. Sheehan, "Reduction of graphene oxide by electron beam generated plasmas produced in methane/argon mixtures," *Carbon*, vol. 48, no. 12, pp. 3382–3390, 2010.

# Bibliography


[1] K. S. Novoselov *et al.*, "Electric field effect in atomically thin carbon films," *science*, vol. 306, no. 5696, pp. 666–669, 2004.

[2] V. Shanmugam *et al.*, "A review of the synthesis, properties, and applications of 2d materials," *Particle & Particle Systems Characterization*, vol. 39, no. 6, p. 2 200 031, 2022.

[3] S. Wang, Y. Yang, J. Liu, L. Chen, S. Liang, and H. Fang, "Unexpected ion sieving in graphene oxide membranes," *The Journal of Physical Chemistry C*, vol. 126, no. 22, pp. 9572–9579, 2022.

[4] Z. Wang *et al.*, "Ion sieving in graphene oxide membrane enables efficient actinides/lanthanides separation," *Nature Communications*, vol. 14, no. 1, p. 261, 2023.

[5] L. Chen *et al.*, "Ion sieving in graphene oxide membranes via cationic control of interlayer spacing," *Nature*, vol. 550, no. 7676, pp. 380–383, 2017.

[6] P. Jia *et al.*, "The combination of 2d layered graphene oxide and 3d porous cellulose heterogeneous membranes for nanofluidic osmotic power generation," *Molecules*, vol. 26, no. 17, p. 5343, 2021.

[7] A. G. Fane, R. Wang, and M. X. Hu, "Synthetic membranes for water purification: Status and future," *Angewandte Chemie International Edition*, vol. 54, no. 11, pp. 3368–3386, 2015.

[8] T. Foller, H. Wang, and R. Joshi, "Rise of 2d materials-based membranes for desalination," *Desalination*, vol. 536, p. 115 851, 2022.

[9] T. Zhao *et al.*, "A review on the recycling of spent lithium iron phosphate batteries," *Journal of Environmental Management*, vol. 351, p. 119 670, 2024.

[10] Y. Yang *et al.*, "A closed-loop process for selective metal recovery from spent lithium iron phosphate batteries through mechanochemical activation," *ACS Sustainable Chemistry & Engineering*, vol. 5, no. 11, pp. 9972–9980, 2017.

[11] M. Wang *et al.*, "Recycling of lithium iron phosphate batteries: Status, technologies, challenges, and prospects," *Renewable and Sustainable Energy Reviews*, vol. 163, p. 112 515, 2022.

[12] M. Anton, *The relation of graphene to graphite.* Wikimedia Commons. `https://pl.wikipedia.org/wiki/Plik:Graphene-graphite_relation.png`, 2009.

[13] D. R. Cooper *et al.*, "Experimental review of graphene," *International Scholarly Research Notices*, vol. 2012, 2012.

[14] A. Dabrowska, M. K. Kurcz, and A. Huczko, *Grafen: otrzymywanie, charakterystyka, zastosowania.* Wydawnictwa Uniwersytetu Warszawskiego, 2018.

[15] Ponor, *Sigma and pi bonds in graphene. sigma bonds result from an overlap of sp2 hybrid orbitals, whereas pi bonds emerge from tunneling between the protruding pz orbitals. for clarity, only a few neighboring pz orbitals are shown*, Wikimedia Commons. https://commons.wikimedia.org/wiki/File:Graphene_-_sigma_and_pi_bonds.svg, 2020.

[16] W. Yu, L. Sisi, Y. Haiyan, and L. Jie, "Progress in the functional modification of graphene/graphene oxide: A review," *RSC advances*, vol. 10, no. 26, pp. 15 328–15 345, 2020.

[17] Iridos, *Graphene oxide. see papers.* Wikimedia Commons. https://commons.wikimedia.org/wiki/File:Graphite_oxide.svg, 2012.

[18] E. Jaafar, M. Kashif, S. K. Sahari, and Z. Ngaini, "Study on morphological, optical and electrical properties of graphene oxide (go) and reduced graphene oxide (rgo)," in *Materials Science Forum*, Trans Tech Publ, vol. 917, 2018, pp. 112–116.

[19] J. W. Suk, R. D. Piner, J. An, and R. S. Ruoff, "Mechanical properties of monolayer graphene oxide," *ACS nano*, vol. 4, no. 11, pp. 6557–6564, 2010.

[20] L. Liu, J. Zhang, J. Zhao, and F. Liu, "Mechanical properties of graphene oxides," *Nanoscale*, vol. 4, no. 19, pp. 5910–5916, 2012.

[21] S. Zhang, H. Wang, J. Liu, and C. Bao, "Measuring the specific surface area of monolayer graphene oxide in water," *Materials Letters*, vol. 261, p. 127 098, 2020.

[22] Z.-S. Wu, W. Ren, L. Gao, B. Liu, C. Jiang, and H.-M. Cheng, "Synthesis of high-quality graphene with a pre-determined number of layers," *Carbon*, vol. 47, no. 2, pp. 493–499, 2009.

[23] A. Jiříčková, O. Jankovskỳ, Z. Sofer, and D. Sedmidubskỳ, "Synthesis and applications of graphene oxide," *Materials*, vol. 15, no. 3, p. 920, 2022.

[24] W. Yu, L. Sisi, Y. Haiyan, and L. Jie, "Progress in the functional modification of graphene/graphene oxide: A review," *RSC advances*, vol. 10, no. 26, pp. 15 328–15 345, 2020.

[25] J. W. M. et al. "11.4: Hydration of ions - chemistry libretexts." (), [Online]. Available: https://chem.libretexts.org/Bookshelves/General_Chemistry/ChemPRIME_(Moore_et_al.)/11%3A_Reactions_in_Aqueous_Solutions/11.04%3A_Hydration_of_Ions (visited on 05/25/2024).

[26] E. Nightingale Jr, "Phenomenological theory of ion solvation. effective radii of hydrated ions," *The Journal of Physical Chemistry*, vol. 63, no. 9, pp. 1381–1387, 1959.

[27] L. Ding *et al.*, "Effective ion sieving with ti3c2t x mxene membranes for production of drinking water from seawater," *Nature Sustainability*, vol. 3, no. 4, pp. 296–302, 2020.

[28] J. Abraham *et al.*, "Tunable sieving of ions using graphene oxide membranes," *Nature nanotechnology*, vol. 12, no. 6, pp. 546–550, 2017.

[29] J. Ran *et al.*, "Non-covalent cross-linking to boost the stability and permeability of graphene-oxide-based membranes," *Journal of materials chemistry A*, vol. 7, no. 14, pp. 8085–8091, 2019.

[30] M. Tagliazucchi and I. Szleifer, "Transport mechanisms in nanopores and nanochannels: Can we mimic nature?" *Materials Today*, vol. 18, no. 3, pp. 131–142, 2015.

[31] M.-L. Bocquet, *Snapshot of graphene oxide in liquid water from molecular dynamics simulation*, Wikimedia Commons. `https://commons.wikimedia.org/wiki/File:Graphene_oxide_in_liquid_water.png`, 2020.

[32] A. Iakunkov and A. V. Talyzin, "Swelling properties of graphite oxides and graphene oxide multilayered materials," *Nanoscale*, vol. 12, no. 41, pp. 21 060–21 093, 2020.

[33] G. Yuan *et al.*, "Ion and molecule sieving through highly stable graphene-based laminar membranes," *The Journal of Physical Chemistry Letters*, vol. 14, no. 7, pp. 1702–1707, 2023.

[34] A. S. Mahadevi and G. N. Sastry, "Cation- $\pi$ interaction: Its role and relevance in chemistry, biology, and material science," *Chemical reviews*, vol. 113, no. 3, pp. 2100–2138, 2013.

[35] P. M. V. Raja and A. R. Barron. "4.3: Raman spectroscopy - chemistry libretexts." (), [Online]. Available: `https://chem.libretexts.org/Bookshelves/Analytical_Chemistry/Physical_Methods_in_Chemistry_and_Nano_Science_(Barron)/04%3A_Chemical_Speciation/4.03%3A_Raman_Spectroscopy` (visited on 05/25/2024).

[36] K. D. Vernon-Parry, "Scanning electron microscopy: An introduction," *III-Vs review*, vol. 13, no. 4, pp. 40–44, 2000.

[37] G. F. Harrington and J. Santiso, "Back-to-basics tutorial: X-ray diffraction of thin films," *Journal of Electroceramics*, vol. 47, no. 4, pp. 141–163, 2021.

[38] A. S. Khune *et al.*, "Highly sensitive, selective, repeatable and flexible chemiresistive no2 sensor based on reduced graphene oxide/free based porphyrin composite," *Journal of Materials Science: Materials in Electronics*, vol. 35, no. 9, p. 672, 2024.

[39] F. T. Johra, J.-W. Lee, and W.-G. Jung, "Facile and safe graphene preparation on solution based platform," *Journal of Industrial and Engineering Chemistry*, vol. 20, no. 5, pp. 2883–2887, 2014.

[40] H. Y. Mohammed, M. A. Farea, Z. M. Ali, S. M. Shirsat, M.-L. Tsai, and M. D. Shirsat, "Poly (n-methyl pyrrole) decorated rgo nanocomposite: A novel ultrasensitive and selective carbon monoxide sensor," *Chemical Engineering Journal*, vol. 441, p. 136 010, 2022.

[41] S. Stankovich *et al.*, "Synthesis of graphene-based nanosheets via chemical reduction of exfoliated graphite oxide," *carbon*, vol. 45, no. 7, pp. 1558–1565, 2007.

[42] M. Baraket, S. Walton, Z. Wei, E. Lock, J. Robinson, and P. Sheehan, "Reduction of graphene oxide by electron beam generated plasmas produced in methane/argon mixtures," *Carbon*, vol. 48, no. 12, pp. 3382–3390, 2010.

**DEPARTMENT OF INDUSTRIAL AND MATERIALS SCIENCE**
**CHALMERS UNIVERSITY OF TECHNOLOGY**
Gothenburg, Sweden
www.chalmers.se


CHALMERS
UNIVERSITY OF TECHNOLOGY